Version of Record: https://www.sciencedirect.com/science/article/pii/S0967063718303042
Manuscript_7d721addf119492647b392b7589d07d4

This information is distributed solely for the purpose of pre-dissemination peer review and must not be disclosed, released, or published until after approval by the U.S. Geological Survey (USGS). It is deliberative and pre-decisional information and the findings and conclusions in the document have not been formally approved for release by the USGS. It does not represent and should not be construed to represent any USGS determination or policy.

Examination of *Bathymodiolus childressi* nutritional sources, isotopic niches, and food-web linkages at two seeps in the US Atlantic margin using stable isotope analysis and mixing models.

Demopoulos, A.W.J., McClain-Counts, J., Bourque, J., Prouty, N., Smith, B.J., Brooke, S., Ross, S.W., Ruppel, C.

ABSTRACT

Chemosynthetic environments support distinct benthic communities capable of utilizing reduced chemical compounds for nutrition. Hundreds of methane seeps have been documented along the U.S. Atlantic margin (USAM), and detailed investigations at a few seeps have revealed distinct environments containing mussels, microbial mats, authigenic carbonates, and soft sediments. The dominant mussel, *Bathymodiolus childressi*, contains methanotrophic endosymbionts but is also capable of filter feeding and stable isotope analysis (SIA) of mussel-shell periostracum suggests that these mussels are mixotrophic, assimilating multiple food resources. However, it is unknown whether mixotrophy is widespread or varies spatially and temporally. We used SIA ($\delta^{13}C$, $\delta^{15}N$, and $\delta^{34}S$) and an isotope mixing model (MixSIAR) to estimate resource contribution to *B. childressi* and characterize food webs at two seep sites (Baltimore Seep; 400 m and Norfolk Seep; 1500 m depths) along the USAM, and applied a linear mixed-effects model to explore the role of mussel population density and tissue type in

© 2019 published by Elsevier. This manuscript is made available under the Elsevier user license
https://www.elsevier.com/open-access/userlicense/1.0/

influencing SIA variance. After controlling for location and temporal variation, isotopic variability was a function of proportion of live mussels present and tissue type. Isotopic differences were also spatially discrete, possibly reflecting variations in the underlying carbon source at the two sites. Low mussel $\delta^{13}C$ values (~ -63‰) are consistent with a dependence on microbial methane. However, MixSIAR results revealed mixotrophy for mussels at both sites, implying a reliance on a mixture of methane and phytoplankton-derived particulate organic material. The mixing model results also reveal population density-driven patterns, suggesting that resource use is a function of live mussel abundance. Mussel isotopes differed by tissue type, with gill having the lowest $\delta^{15}N$ values relative to muscle and mantle tissues. Based on mass balance equations, up to 79% of the dissolved inorganic carbon (DIC) of the pore fluids within the anaerobic oxidation of the methane zone is derived from methane and available to fuel upper slope deep-sea communities, such as fishes (*Dysommina rugosa* and *Symphurus nebulosus*), echinoderms (*Odontaster robustus*, *Echinus wallisi*, and *Gracilechinus affinis*), and shrimp, (*Alvinocaris markensis*). The presence of these seeps thereby increases the overall trophic and community diversity of the USAM continental slope. Given the presence of potentially hundreds of seeps within the region, primary production at seeps may serve as an important, yet unquantified, energy source to the USAM deep-sea environment.

Key words: stable isotopes, MixSIAR, *Bathymodiolus childressi*, methane seeps, chemosynthesis, mixotrophy, trophic ecology

Introduction:

Hundreds of methane seeps have been discovered along the U.S. Atlantic margin (USAM) north of Cape Hatteras (Skarke et al., 2014). Site-specific characterizations at a few of the newly discovered seeps (Quattrini et al., 2015; Ross et al., 2015; Prouty et al., 2016a; Bourque et al., 2017; McVeigh et al., 2018) revealed communities composed of microbial mats and mussel beds that are patchily distributed and range in size from several cm (small mats and few individuals of mussels) to large expanses of mussel beds (Quattrini et al., 2015; CSA Ocean Sciences Inc et al., 2017). These seep inhabitants are associated with specific locations of gas emissions (Ruppel et al. 2017; McVeigh et al., 2018). The dominant mussels at U.S. Atlantic seeps are from the bathymodiolin group, known to harbor endosymbiotic chemoautotrophs and methanotrophs in their gills (Childress et al., 1986; Cavanaugh et al., 1987; Duperron et al., 2009). They are also able to filter feed (Page et al., 1990; 1991), potentially providing mussels with essential nitrogen (Pile and Young, 1999). Mussel sizes varied within these beds, suggesting continual recruitment of mussels over time (Quattrini et al., 2015). Whereas *Bathymodiolus heckerae* occurs at the Blake Ridge seep (Van Dover et al., 2003), *B. childressi* was recently identified as the dominant mussel from two seep sites near Baltimore and Norfolk canyons (Coykendall et al. 2019). *Bathymodiolus childressi* hosts methanotrophic endosymbionts that fix methane (Brooks et al., 1987; Duperron et al., 2007, 2013; Kellermann et al., 2012), as well as potentially hosting sulfur-oxidizing thiotrophic symbionts (Assie et al., 2016). However, the relative role of chemoautotrophy, methanotrophy, and heterotrophy (e.g., energy from filter feeding) for U.S. Atlantic populations of *B. childressi* mussels is unknown.

Mussel species and their presence/absence, abundance, and spatial extent provide clues about the source and persistence of reduced compounds (e.g., methane, sulfur) to fuel endosymbionts in the local environment (e.g., Duperron et al., 2013; Laming et al., 2018), as well as larger-scale

processes that influence carbon and nitrogen pools (Becker et al., 2010). Therefore, seep bivalves are associated with specific habitats, and their distribution is influenced by physico-chemical conditions (Van Dover, 2000; Heyl et al., 2007; Duperron et al., 2013). Dietary sources of sulfur for these mussels are unknown (Dattagupta et al., 2004), but *B. childressi* sulfur isotopes from Gulf of Mexico (GOM) seeps suggest seawater sulfate ($\delta^{34}S$ ~ 20‰) as a dietary source (Brooks et al., 1987; Riekenberg et al., 2016). Recent work by Coykendall et al. (2019) confirmed the presence of a single Type 1 methanotrophic symbiont (Gammoproteobacteria) within mussel gill tissue from Baltimore and Norfolk seeps. However, mussels within the Norfolk seeps also contained epibiotic sulfur-oxidizing epsilonproteobacteria (Coykendall et al. 2019), consistent with sulfur-oxidizing epsilonproteobacterial sequences in *Bathymodiolus* species from the GOM (Assie et al., 2016) and depleted gill $\delta^{34}S$ values from a few USAM mussels (Prouty et al, 2016a). Therefore, the degree to which sulfur oxidizers provide energy to the mussels is unknown (Assie et al., 2016), may be site specific, and could be related to mussel health condition (e.g., Dattagupta et al., 2004). The overall seep trophic ecology and important food resources utilized by mussels and seep associates at these newly discovered seeps have yet to be examined.

Stable isotope analysis (SIA) is useful for discerning complex food webs, particularly in remote environments like the deep sea and particularly at seeps (see reviews by Levin, 2005, Van Dover, 2007, Levin et al., 2016). Photosynthetically derived material has a distinct $\delta^{13}C$ range (-25 to -15‰), whereas microbial methane present at seeps is isotopically depleted in ^{13}C (<-50‰) and is associated with low $\delta^{13}C$ values for fauna housing chemoautotrophic and methanotrophic endosymbionts and heterotrophic fauna that consume seep-derived organic matter (e.g., free-living bacteria; Fry and Sherr, 1984; Van Dover, 2007; Thurber et al., 2010).

Microbes involved in anaerobic oxidation of methane (AOM) via sulfate reduction kinetically discriminate for the lighter isotopes during metabolism, resulting in mussel tissue that is isotopically depleted in ^{13}C and ^{34}S. Thus, large variability in sulfur and carbon isotopic composition of mussels could be used to reveal thiotrophic and methanotrophic symbioses. Because isotopes are assimilated into tissues with different turnover times (Deudero et al., 2009), SIA can provide temporally and spatially integrated trophic estimates used to understand and define trophic linkages among species and communities (Dattagupta et al., 2004).

Seep fluids in the USAM originate from various sources, fueled by methane generated largely from microbial decomposition of organic matter, which is also referred to as microbial or biogenic methane (Paull et al., 1995; Prouty et al., 2016a; Pohlman et al., 2017). The $\delta^{13}C$ of methane ranges between -109 to -61.1‰ at depths of 450 - 2200 m at seeps near Baltimore Canyon, Cape Fear, and Blake Ridge (Paull et al., 1995, 2000; Pohlman et al., 2015, 2017). Corresponding $\delta^{13}C$ measurements of soft tissues from chemosynthetic mussels at Blake Ridge ($\delta^{13}C$ = -55.7 ± 1.9‰; Van Dover et al., 2003) and mussel shell periostracum and authigenic carbonate from seeps near Norfolk and Baltimore canyons ($\delta^{13}C$ ~ -49 to -47‰ [carbonate], -57‰ [periostracum]; Prouty et al., 2016a) provide a proxy for determining the carbon source fueling these seeps and are also consistent with a microbial methane source (Brooks et al., 1987). However, while methane may be a dominant carbon source within these seeps, it is unclear whether the source contribution varies spatially or temporally within and across these seep environments. Comparisons of multiple mussel tissues (gill, mantle, and muscle) that have different turnover rates can provide insight into temporal variability in the methane source assimilated by the tissues and among different mussel populations.

For this study, we used SIA and mixing models (MixSIAR) to estimate the relative contribution of different energy substrates and address the role of chemoautotrophy, methanotrophy, and heterotrophy to *B. childressi* populations. Here, we used mussel tissue $\delta^{13}C$ to infer stable isotope composition of the methane source and $\delta^{34}S$ to differentiate between thiotrophic and methanotrophic nutritional modes. Linear mixed effects models (LMMs) were used to examine the role of tissue type (mantle, gill, muscle) and mussel population density in isotope variability within the mussels, while controlling for sampling location and temporal variation. Lastly, we used stable carbon and nitrogen isotopes to examine the overall seep food web at two sites.

This study is the first to characterize the isotopic compositions of gill, muscle, and mantle tissues of *B. childressi* at two primary seep sites within the USAM. By integrating metrics of seepage (i.e., $\delta^{13}C$ values), mixing models, and estimates of mussel population densities, this study provides insight into whether mussels exhibit trophic plasticity and niche partitioning over time, across different sizes of mussel habitats and environmental conditions, which would enable survival in areas with fluctuating energy sources (Riekenberg et al., 2016, 2018). For example, variability in mussel stable isotopes across tissues could reflect spatio-temporal variability in the methane flux and source. By examining the isotopic composition of seep associates, our goal is to characterize deep-sea food webs at these newly discovered seeps. Ultimately, this research helps to constrain the role of seeps in overall biological productivity along the USAM and their potential influence in global elemental cycling.

2.0 Methods:

2.1 Study site

Two large USAM methane seep environments were investigated in 2012, 2013, 2015, and 2017 (Fig. 1). Seeps near the southern edge of Baltimore Canyon (BCS) are located on the continental slope, between 366-450 m (Bourque et al., 2017). Norfolk Canyon seeps (NCS) are deeper (1457-1602 m) than BCS and located about 20 km south of the thalweg of Norfolk Canyon. For more detailed site descriptions, see Bourque et al. (2017). *Bathymodiolus childressi* occurs at both seep sites (Coykendall et al., 2019). These seeps contain areas of large and small mussel patches (living and dead), microbial mats, and carbonate rocks (Bourque et al., 2017). NCS had more variable mussel patch sizes than BCS, with mussel populations ranging in size from small patches of a few individuals to densely packed fields that were several hundred square meters (Fig. 1; Demopoulos et al., 2014; CSA Ocean Sciences Inc et al., 2017).

2.2 Sample collection

Collections occurred during four research cruises in 2012, 2013, 2015, and 2017 (Supplementary Table 1). Multiple gear types, including push cores, remotely operated vehicle (ROV) suction and grab samples, and Niskin bottles were used to sample sediments, fauna, and seawater. Water samples were collected at various water depths using Niskin bottles mounted on the vessel's conductivity-temperature-depth (CTD) rosette and were filtered for particulate organic matter (POM; 0.7 μm GFF). *In situ* collections were conducted using the ROVs *Kraken 2* (University of Connecticut, 2012), *Jason II* (Woods Hole Oceanographic Institute [WHOI], 2013), HOV *Alvin* (WHOI), and *Global Explorer* (Oceaneering, 2017). Macrobenthic invertebrates and fishes were collected using either the suction systems or the manipulator arms on the ROVs, while sediments were collected using T-handle push cores (31.7 cm^2 × 30 cm) operated by the manipulator arm. Additional water samples were collected using Niskin bottles attached to the ROVs. Mussels were collected in a range of habitat patch sizes, whereas fish and non-mussel invertebrate

collections were opportunistic. Feeding groups were assigned to fauna based on a classification devised by Demopoulos et al. (2017).

2.3 Image analysis to estimate mussel population density

The ROVs conducted slow speed (0.5 kts, 0.26 m/s) video transects of variable lengths across multiple habitat types. During transects, the video cameras were set on wide angle and positioned to record in front of the ROV at a consistent angle. The science cameras on the ROVs included an Insite Mini-Zeus HD video camera (*Jason*), Kongsberg OE14-502 HD (*Kraken*), and Ocean Pro HD (*Global Explorer*), all with scaling lasers (10 cm apart). Each image captured from the video was georeferenced for habitat analysis. Only video collected while the vehicles were in transect configuration with lasers on and with adequate visibility to enable habitat and faunal descriptions was used in the analysis; other sections of the video were excluded. The video and/or still images taken during sample collection were split into two categories representing low (<25%) and high (25-100%) live mussel population density.

2.4 Stable isotope analysis

Dissections of fish and invertebrate tissues occurred at sea prior to processing for stable isotopes. For consistency, tissue was removed from similar body regions based on taxa (e.g., muscle from the dorsal region of fishes; caudal tissue of shrimps; leg muscle for crabs; mantle, gill, and adductor muscle for molluscs; legs for brittle stars; gonads for urchins; and polyps for corals). Tissue samples were dried to a constant weight at 50° C to 60° C, ground to a fine powder, and weighed into tin capsules. Invertebrate samples were acidified with 10% platinum chloride to remove inorganic carbon. POM filters were dried and treated with 1.0 N hydrochloric acid, then scraped into tin boats. Sediment samples were homogenized prior to drying and

acidified with 1.0 N phosphoric acid before weighing into tin boats. Samples were analyzed for $\delta^{13}C$ and $\delta^{15}N$ composition referenced to Vienna PeeDee Belemnite and atmospheric nitrogen gas, respectively. Analyses were conducted at Washington State University using a Costech (Valencia, USA) elemental analyzer interfaced with a GV instruments (Manchester, UK) Isoprime isotope ratio mass spectrometer. Sulfur isotopes were analyzed at Washington State University Stable Isotope Core Laboratory using a ECS 4010 Costech elemental analyzer coupled with a Delta PlusXP Thermo-Finnigan continuous flow isotope ratio mass spectrometer. Sulfur isotope ratios ($\delta^{34}S$) were referenced relative to VCDT (Vienna Canyon Diablo Troilite). Precision of $\delta^{13}C$ and $\delta^{15}N$ was verified using egg albumin calibrated against National Institute of Standards reference materials. Analytical accuracy of $\delta^{34}S$ was verified using an internal lab standard referenced to International Atomic Energy Agency standards. Reproducibility of all isotopes was monitored using organic reference standards and sample replicates (Fry, 2007; Demopoulos et al., 2017) within ±0.2‰ for all three isotopes. Isotope ratios were expressed in standard delta notation, $\delta^{13}C$, $\delta^{15}N$, and $\delta^{34}S$ as per mil (‰). Reported $\delta^{13}C$ values were taken from analyzed acidified samples and $\delta^{15}N$ and $\delta^{34}S$ values from non-acidified samples to avoid the potential artifact associated with acidification (Pinnegar and Polunin, 1999). Voucher specimens were preserved at sea in 10% formalin-seawater following isotope dissections and later identified to the lowest possible taxon in the lab. Several mussel samples dissected for isotope analysis were photographed with a ruler, and mussel-shell length estimates (mm) were made using image analysis.

2.5 Statistical analysis

Correlations of isotope data ($\delta^{13}C$, $\delta^{15}N$, and $\delta^{34}S$) were tested using Pearson Product Moment Correlation for subsets of the data within sites and tissues, and with mussel size. LMMs

were used to examine whether there were tissue, sampling date, and proportion of live mussel differences in $\delta^{13}C$, $\delta^{15}N$, and $\delta^{34}S$ values. We built a model set for each isotope (Supplemental Tables 2-4) by first constructing a fully saturated model that estimated the isotopic value as a three-way interaction between tissue, year, and proportion live mussel, along with the random intercept. Details regarding model analysis are found in Supplementary Materials.

In order to estimate mussel isotopic niche size, standard ellipse areas corrected for sample size (SEA_C) and the Bayesian SEA (SEA_B) were calculated using the SIBER packages (Jackson et al., 2011; Demopoulos et al., 2017, 2018) in R version 3.5.0 (R Development Core Team, 2018) for mussel populations based on tissue, site, and mussel density. Specific details regarding the niche analysis can be found in the Supplemental Materials. SEA_B can be used to approximate trophic diversity and variance in available resources at the baseline. SIBER was also used to examine mussel trophic structure by calculating the following Layman metrics (Layman et al., 2007; Jackson et al., 2011; Demopoulos et al., 2017, 2018): $\delta^{13}C$ range (CR), $\delta^{15}N$ range (NR), mean distance to centroid (CD), mean nearest neighbor distance (MNND) and standard deviation of nearest neighbor distance (SDNND). Food-web length is estimated by NR, while CR represents the overall food-web width, providing a diversity metric of available basal sources and/or variation in the isotope ranges of these sources. CD estimates overall trophic diversity and is influenced by the degree of species spacing in isotope space. MNND estimates trophic redundancy, where lower numbers indicate food webs with a high proportion of species that have similar trophic ecologies and hence, higher trophic redundancy. Low SDNND values represent even distribution of trophic niches within isotope space.

The MixSIAR stable isotope mixing model (Stock and Semmens, 2016) was used to estimate proportional contributions of different food resources to the mussels' diet. The sources

were inferred using the mussel stable isotope data and are consistent with the known ecology of *B. childressi* (e.g., Riekenberg et al., 2016). We used a similar approach to that described by Riekenberg et al. (2016) to identify inferred food resources to *B. childressi*, as well as the general guidance to mixing model applications suggested by Phillips et al. (2014). Specific details regarding the analysis can be found in the Supplemental Materials. MixSIAR analysis was run using muscle tissue, with site (BCS, NCS) as a fixed effect for an initial model run. Following the outcome of the LMMs, we re-ran the MixSIAR to estimate resource contribution to mussels as a function of mussel population density (high or low) by muscle tissue for each site. Both mussel population density and site were included as fixed effects in this follow-up model. Because there is potentially an isotopic contribution of the symbionts to gill and mantle tissues (Streams et al., 1997), we chose to analyze only muscle tissue in MixSIAR.

3. Results

3.1. Isotope results

A total of 564 samples (312 from BCS and 252 from NCS, Tables 1 and 2; Fig. 2), representing 6 phyla, were analyzed. Bottom water POM at seeps was depleted in ^{13}C and ^{15}N relative to bottom POM collected in the non-seep stations (Table 2). Stable carbon isotope values of many of the fauna fell between two primary endmembers, phytoplankton ($\delta^{13}C$ > -25‰) and methane-derived carbon (< -40‰). Microbial mats, which were only sampled at NCS, had similar $\delta^{13}C$ values (-29.4‰) relative to organic matter from surface sediments (-30.7 ± 8.2‰).

3.2. Mussel stable isotope characteristics

The three different types of *B. childressi* tissues (mantle, gill, and muscle) had overlapping isotope values for both $\delta^{13}C$ and $\delta^{15}N$ (Supplemental Fig. 1, Table 1), and isotopic differences exist between populations of mussels found at the two sites and among tissues sampled. For the BCS populations, mantle had the lowest and muscle the highest $\delta^{13}C$ values, and muscle and mantle both had a negative skew (Supplemental Fig. 1, Supplemental Table 5). Gill had the lowest $\delta^{15}N$ values compared to mantle and muscle, and gill and mantle $\delta^{15}N$ data had a positive skew. There were no observable among-tissue differences in $\delta^{34}S$, but all tissue $\delta^{34}S$ data had a negative skew. For NCS populations, muscle was higher in $\delta^{13}C$ relative to gill and mantle, with gill having a negative skew. Muscle and gill tissues had the highest and lowest $\delta^{15}N$ values, respectively. There was a slight multimodal distribution with a negative skew in muscle $\delta^{15}N$ at NCS, with peaks at ~0 and 3‰. There were no observable among-tissue differences in $\delta^{34}S$, and none of the data had skew.

Across both sites, significant correlations occurred between $\delta^{13}C$ and $\delta^{15}N$ values for mantle tissue (ρ=0.236, p=0.005). These significant correlations are consistent with the linkages between food assimilation and resource use and corresponding isotope values, providing support for the application of mixing models (Riekenberg et al., 2016), including MixSIAR.

Correlation analysis between size and tissue isotopes was conducted to identify if mussel individual size (length) played a role in isotopic composition. Mussel length measurements were recorded from a subset of specimens from 2012, 2013, and 2017. Sizes ranged from 58-104 mm for BCS (n=24) and 27-118 mm for NCS (n=33). For NCS, there was no significant correlation between mussel size and either $\delta^{13}C$, $\delta^{15}N$, or $\delta^{34}S$ for any of the tissues. For BCS mussels, gill and mantle $\delta^{15}N$ were significantly correlated with mussel size (gill: ρ=0.552, p=0.004; mantle: ρ=0.416, p=0.043). However, mussel length was not correlated with $\delta^{13}C$ for any tissue.

3.3. Role of site, habitat, tissue type, and time in mussel isotope variance

Using LMMs, we addressed which factors, including associated interactions, drive isotope variability across populations (% live mussels, tissue type, site [BCS vs. NCS], and sampling year). For $\delta^{13}C$, the top model was the full model, which had all 3 fixed factors and all possible 2-way and 3-way interactions [R^2(marginal)=0.21, R^2(conditional)=0.45] (Supplemental Table 2). The 2nd best model within 2 ΔAICc of this top model included all three factors and 2 interactions: live mussel x year and tissue x year, and the 3rd best model included all 3 factors, plus the interactions: live x site and tissue x year. For $\delta^{15}N$, the top model included all 3 factors and the interaction: live mussel x year [R^2(marginal)=0.32, R^2(conditional)=0.76] (Supplemental Table 3). Lastly, using the subset of data analyzed for $\delta^{34}S$ from a single year, there were three models within 2 ΔAICc values. The top model included two predictors: live mussel, tissue, and their interaction [R^2(marginal)=0.13, R^2(conditional)=0.77] (Supplemental Table 4). The 2nd model included live mussel only and 3rd highest model included live mussel and tissue type. For each isotope, the top models within 2 ΔAICc were averaged and predictions were estimated. The average trends showed that regardless of tissue type, areas with more live mussel (categorized as "high") had lower $\delta^{15}N$ values, nominally lower $\delta^{13}C$ values (particularly for samples collected in 2013; see Supplemental Fig. 2), and higher $\delta^{34}S$ values (Figs. 3 and 4). The top models for all three isotopes showed a substantial difference between the R^2(marginal) and the R^2(conditional), indicating that the random effect explained a large proportion of the variance. On average, NCS was slightly more enriched in the heavy isotope across all three elements (Supplemental Fig. 3).

3.4. Isotope niche area estimates

Because the LMM analysis indicated that the mussel isotope data are a function of tissue type (mantle, gill, and muscle) and relative mussel density (high and low), we used SIBER analyses to determine whether the two mussel populations (BCS and NCS) were isotopically different in terms of overall niche space, based on tissue type and density. The standard ellipse areas (SEA_C and SEA_B) for gill samples from NCS mussels were higher than from BCS (Table 3, Supplemental Fig. 4). However, there was no difference in SEA_B in the rest of the tissue pairs (muscle and mantle). The greatest overlap between sites in SEA_C was for gill tissue, followed by mantle, then muscle tissue. Within sites, SEA_B for gill was less than mantle for both sites (NCS: $p=0.03$, BCS: $p=0.003$). In terms of overall trophic diversity using data for all tissues, mussels from BCS had a higher CR than from NCS (Table 4, $p=0.0005$), indicating a greater resource pool, diversity of available food resources, and/or greater variability in the isotope values of those resources. In contrast, NCS mussels had higher NR than BCS mussels ($p=0.002$), implying a greater diversity of nitrogen sources and/or variability of the isotopic values of available nitrogen sources. There was no difference in CD, consistent with similar overall trophic diversity between the two populations of mussels. Lower NND for NCS ($p=0.048$) indicates greater overall trophic redundancy and overlap in feeding niches.

In order to identify whether mussels have different sized isotopic niches with different mussel densities (low or high), based on the LMM analysis, we examined SEA_C and SEA_B for NCS and BCS populations relative to mussel densities (separately by tissue). There were no differences in SEA_B values as a function of mussel densities at BCS, regardless of tissue type (Supplementary Table 6). However, gill tissues from NCS populations had significantly higher SEA_B values in high density mussel beds compared to the lower density areas.

3.5. Mixing model results (MixSIAR)

Isotope results suggested that mussels assimilate a variety of food resources (Table 1, Supplemental Figs. 1 and 3). Patterns in mussel stable isotope data supported our decision to use MixSIAR to estimate resource contributions based on three criteria (Riekenberg et al., 2016), as follows: 1) the large standard deviation in the isotope data for the mussel tissues (Table 1) supports the hypothesis that mussel nutrition was derived from multiple sources (Barnes et al., 2008; Riekenberg et al., 2016), 2) the muscle $\delta^{15}N$ data were multimodal, also indicative of assimilation of multiple sources (Supplemental Fig. 1), and 3) the significant correlations among mussel isotopes was consistent with the values being tied directly to food resources.

While it is difficult to quantify all the possible food sources at these two different sites (NCS and BCS), four sources (Table 5) were chosen because they bounded the isotope data with a tight fit (Supplemental Fig. 5; e.g., Phillips et al., 2014), they represent feasible sources available in the environment, and all four sources were based on actual measurements available for the region. However, because site-specific source values were not available for all four sources, the same isotopic values for sources were used for both sites, and the model was run to estimate the proportional contribution of each of these sources to muscle tissue by location (BCS or NCS). The four sources are further defined as follows (Table 5): a detrital source of phytoplankton based on average values from two sediment traps deployed at 603 m (Baltimore) and 1364 m (Norfolk) depth ($\delta^{13}C$: -22.3 ± 0.2‰, $\delta^{15}N$: 5.0 ± 0.1‰; Mienis et al., 2017; Prouty et al., 2017) and published seawater sulfate values for the region ($\delta^{34}S$: 20.5 ± 0.2‰; Heyl et al., 2007). The contribution of sulfur-oxidizing (thiotrophic) microbes to mussel diets was estimated using published sulfur-oxidizing microbial isotope values from the GOM (*Beggiatoa*: $\delta^{13}C$: -32.8 ± 1.8‰, $\delta^{15}N$: -3.5 ± 2‰; Demopoulos et al., 2010), and a source $\delta^{34}S$ value indicative of seep

hydrogen sulfide ($\delta^{34}S$: -6.6 ± 1.4‰; Heyl et al., 2007). Because only one microbial sample was available from NCS (Table 2), we used the published values to provide a better-resolved estimate of this resource, including error estimates. Based on the shape of the tetrahedron and spread of $\delta^{13}C$ data, we assumed two possible methane sources from two separate methane pools: Seep-1 and Seep-2. Seep-1 had very low $\delta^{13}C$ (-100.4 ± 7.6‰) values based on $\delta^{13}C$ from porewater methane measured in the region between Baltimore and Norfolk canyons (Pohlman et al., 2017), low $\delta^{15}N$ from microbial samples (-3.5 ± 2.0‰; Demopoulos et al., 2010), and published $\delta^{34}S$ seawater sulfate values (20.5 ± 0.2‰; Heyl et al., 2007). Seep-2 had slightly higher $\delta^{13}C$, based on average methane values from BCS bottom water (-68.2 to -69.6‰; Pohlman et al., 2015) and porewater from cores collected at Blake Ridge (PC3: -65.1‰; Paull et al., 1995). For this second methane source, we assumed a higher $\delta^{15}N$ value based on sediment samples collected at BCS and NCS (4.8 ± 1.2‰), and low $\delta^{34}S$ values indicative of seep sulfur (-6.6 ± 1.4‰; Heyl et al., 2007).

The proportion of the diet for each of the four endmembers at NCS and BCS was similar (Fig. 5). For BCS, Seep-1 yielded the highest contribution to muscle tissue (median: 32%, range 25-39%), followed by phytodetritus (23-38%), Seep-2 (21-43%), and thiotrophic microbes (0.1-16%). The sum of the two methane-derived seep sources (1 and 2) exceeded all other sources (range: 46-82%). For NCS, phytodetritus (median: 42%) and Seep-1 (37%) had the highest contribution, followed by Seep-2 (median: 20%, 12-20%) and thiotrophic microbes (median: 1.5%, 0.1-6.9%).

Because the covariate for density of mussels (low vs. high) improved the fit of the LMMs, we re-ran the MixSIAR analysis using the same four sources as above, to examine possible differences in resource contribution based on relative abundance of live mussels. This

analysis only included the $\delta^{13}C$ and $\delta^{15}N$ data because there was not sufficient replication within these mussel categories for $\delta^{34}S$ (BCS: N_{low}= 6 and N_{high}=4, NCS: N_{low} = 4 and N_{high} = 6 for low and high categories, respectively). For NCS, high density mussels had the highest contribution of Seep-2 (Fig. 6), followed by similar proportions of Seep-1, thiotrophic microbes, and phytodetritus. For low density mussels, the pattern was similar, but the contribution of phytodetritus and Seep-1 was higher than in the high-density mussel beds. Contribution from thiotrophic microbes was low overall, regardless of mussel densities. For BCS low density mussel beds, Seep-1 and phytodetritus yielded the highest contributions, followed by Seep-2 and thiotrophic microbes. There appeared to be a slightly higher contribution of Seep-2 in high density mussel beds compared to low-density mussels, but credible intervals overlapped. See supplementary information for more details regarding MixSIAR assumptions.

3.7. USAM seep food webs

In addition to *B. childressi*, other taxa collected at the BCS that exhibited $\delta^{13}C$ values indicative of utilizing chemosynthetic production (-75 to -28‰) included the fishes *Dysommina rugosa* and *Symphurus nebulosus*, and the asteroid *Odontaster robustus* (Fig. 2). *Dysommina rugosa* and *S. nebulosus* had a wide range in isotope values. Several other taxa, including mobile species (mesopelagic fishes, several crustaceans), and suspension feeders (e.g., sessile coral, zoanthid, and anemone taxa) collected in proximity to the BCS were enriched in ^{13}C relative to *B. childressi, D. rugosa, S. nebulosus,* and *O. robustus*, (Table 2; Fig. 2), consistent with reliance on phytodetritus as a primary carbon source. Although fewer taxa were collected and analyzed from NCS, all of the taxa analyzed exhibited $\delta^{13}C$ values consistent with utilizing a chemosynthetic derived food source (Table 2; Fig. 2), including the one *B. heckerae* collected.

4. Discussion

4.1. Identification and availability of *methane*

Previous work along the USAM indicates that microbial methane is the dominant carbon source at the Baltimore and Norfolk seep sites (Prouty et al., 2016a). Therefore, gill tissue $\delta^{13}C$ values from these seeps should reflect a similar methane-carbon source at both sites with little isotopic fractionation associated with methanotrophic endosymbionts. All mussel tissues from both sites had $\delta^{13}C$ values (Table 1) that overlap with bottom water methane $\delta^{13}C$ values (-67.6 ‰, Pohlman et al., 2015), with some tissue-specific differences. These differences may reflect different composition and concentrations of lipids, carbohydrates, and proteins, as well as fractionation that occurs within the sediments due to microbial activity (e.g., Becker et al., 2010). For example, low $\delta^{13}C$ values might be associated with the contribution of lipids (e.g., Post et al., 2007). The mussel $\delta^{13}C$ data presented here were not lipid corrected because specific mathematical lipid correction factors for deep-sea chemosynthetic mussels do not exist. Depleted ^{13}C values of mantle and corresponding high C:N values (> 5, Table 1) are consistent with higher amounts of lipids and carbohydrates, and consequently, lower proportional contributions of protein, known for mussel mantle tissues (Riou et al., 2010). In contrast, muscle tissue C:N values remained low (mean: 4.0) with little variation, consistent with higher protein (and hence, higher N) content of adductor muscle. Thus, despite subtle differences among tissues, mussel isotopic composition is consistent with assimilation of microbial methane.

Stable carbon isotope data from this study also enable estimates of available microbial methane as a food source within the zone of AOM (e.g., Feng et al., 2015). Assumptions for this estimate are that the $\delta^{13}C$ of authigenic carbonate represents a mixture of seawater DIC and methane (Prouty et al., 2016b; 47.3 ± 0.16‰ (NCS) and -49.2 ± 0.21‰ (BCS), the $\delta^{13}C$ values

of *B. childressi* reflect those of ascending methane (as discussed above), and seawater DIC is 0.56‰ (BCS) and 0.47‰ (NCS) (Prouty et al., 2016b). Based on a mass balance calculation, 76% (NCS) and 79% (BCS) of the DIC of the pore fluids within the shallow AOM zone is derived from microbial methane and the rest from seawater DIC. This calculation assumes that the authigenic carbonate $\delta^{13}C$ integrates the $\delta^{13}C$ signature of the available DIC pool. Given that there is a small carbon isotopic fractionation between carbonate and bicarbonate during the precipitation of calcium carbonate minerals (~2.7‰; Romanek et al., 1992), this would lead to an underestimate in the fractional contribution of methane. In other words, the actual isotopic value of DIC pool may be more depleted than the carbonate value used in the calculation, so the percent contribution of microbial methane may be even greater. With both seep sites covering a large areal extent of seafloor (CSA Ocean Sciences Inc. et al., 2017), our results suggest that methane seepage on the USAM provides significant amounts of potential carbon energy to fuel upper slope deep-sea communities, including methane that transferred into mussel tissue biomass, which is then available as a food source to some heterotrophic species (e.g., fishes and sea stars) found within the seep environment (Fig. 2).

4.2. Dual symbioses (methanotrophs vs. thiotrophs)

As discussed above, methane-derived seep sources provided the greatest contribution to the diet of the NCS and BCS mussels. However, MixSIAR results estimated a small contribution from thiotrophic microbes (0.1-16%), with assimilation potentially derived from sulfur-oxidizing epsilonproteobacterial ectobionts (e.g., Assie et al., 2016; Coykendall et al., 2019), and/or through consumption of free-living sulfur oxidizers. Animals with sulfide-oxidizing (thiotrophic) symbionts typically record the $\delta^{34}S$ of the substrate used by their symbionts (Vetter and Fry

1998). In contrast, animals with methanotrophs, as well as those without methanotrophic symbionts, integrate seawater $\delta^{34}S$ (Brooks et al., 1987; Duperron et al., 2011). Sources of sulfur are additionally influenced by biogeochemical cycling within the seep environment. Little to no fractionation in $\delta^{34}S$ occurs during sulfide oxidation by chemoautotrophic bacteria (Fry et al., 1983; Vetter and Fry, 1998; Canfield, 2001), with little subsequent isotopic fractionation of sulfur during assimilation by the mussel tissues. Consistent with Prouty et al. (2016a), the $\delta^{34}S$ of *B. childressi* tissues were mostly positive, but depleted relative to seawater sulfate (20‰; Heyl et al., 2007), indicating possible mixed reliance on seawater sulfate and ^{34}S-depleted sulfur from AOM reactions (e.g., Vetter and Fry, 1998; Yamanaka et al., 2003), including potentially thiosulfate (Chambers and Trudinger, 1979; Habicht et al., 1998). Specifically, thiotrophic symbionts (e.g., epibionts) and/or consumption of free-living sulfide oxidizers via filter feeding (Yamanaka et al., 2003; 2015) represent possible mechanisms for acquiring depleted sulfide (Becker et al., 2014). While our study lacks *in situ* measurements of $\delta^{34}S$ (e.g., sediment porewater) to provide context, based on the results of McVeigh et al. (2018) and Heyl et al. (2007) at other seeps along the USAM, there is sufficient hydrogen sulfide to fuel thiotrophs. Given that sediment $\delta^{34}S$ values range from 2.4 to 5.5‰ (Prouty et al., 2016ab), assimilating free-living thiotrophic bacteria is a feasible way to obtain the light ^{34}S incorporated into mussel tissues. Building upon previous work, results from this study using MixSIAR stable isotope mixing model indicate that the estimated contribution from thiotrophic endmembers was low overall, highlighting the dominant role of methanotrophs in *B. childressi*.

4.3 Role of mixotrophy

While *B. childressi* harbors methanotrophic endosymbiotic bacteria, and growing evidence supports the presence of thiotrophic episymbionts (Assie et al., 2016), *B. childressi* is also capable of filter feeding since it maintains a functional gut (Page et al., 1990). Examining $\delta^{15}N$ values from different mussel tissues provides insight into the relative contribution of heterotrophy to mussel nutrition. Nitrogen isotope values are comparable to *B. childressi* values from the GOM (Brooks et al., 1987; Riekenberg et al., 2016). Mussel populations from the GOM supplement nitrogen requirements through selective feeding on nitrogen-rich bacterioplankton, based on variability in tissue $\delta^{15}N$ (Pile and Young, 1999). However, BCS and NCS tissue-$\delta^{15}N$ values were lower than those in the animals reliant on phytodetritus-based food webs in nearby Baltimore and Norfolk canyons (> 5‰; CSA Ocean Sciences Inc et al., 2017; Demopoulos et al., 2017) and lower than $\delta^{15}N$ values of sediments (4.8‰) and bottom POM (3 [NCS] and 6 [BCS] ‰, Table 2). This suggests that the $\delta^{15}N$ derived from filter feeding on suspended material could represent a small fraction of their assimilated diet. MixSIAR results were also consistent with mussel reliance on phytodetritus to a degree. Mussel tissues with slightly negative or low $\delta^{15}N$ values (e.g., close to zero) may result from moderate discrimination of nitrogen sources at high concentrations (Lee and Childress, 1996). Therefore, low $\delta^{15}N$ values may be derived from a local nitrogen source (e.g., activity of autotrophic bacteria, Becker et al., 2010, 2014; Rodrigues et al., 2013; Feng et al., 2015). Likewise, dietary contributions from free-living microbes are also possible with mussel $\delta^{13}C$ values reflecting consumption of free-living methanotrophic bacteria through filter feeding.

Assimilation of isotopically light nitrate or ammonium by the symbionts (Rodrigues et al., 2013) may also explain the low mussel $\delta^{15}N$ values. *Bathymodiolus childressi* can assimilate ammonium, nitrate, and free amino acids (Lee et al., 1992), with assimilation of ammonium and

nitrate specifically occurring in the symbiont-containing tissue (e.g., gills and mantle). Gill tissues, known to host endosymbionts, had the lowest $\delta^{15}N$ (-2.2 to 3.5‰), potentially due to limited fractionation of N from its source (e.g., whether ammonium, nitrate, or both) to assimilated nitrogen in the gill. Mantle tissues may also contain symbionts (Streams et al., 1997), and their $\delta^{15}N$ values were intermediate between gill and muscle (Table 1, Supplemental Fig. 1), possibly reflecting fractionation associated with isotopic routing between tissue types and/or contribution from potential endosymbionts. Similar enrichment between mantle and gill tissues was reported for *B. heckerae* (Van Dover et al., 2003), which is consistent with these mussels primarily relying on organic matter provided by the gill symbionts.

4.4. Isotopic niches and resource contributions to mussels

Differences among isotopes and between isotopic niches (SEA_B) by location (between sites or among individuals within a same population) may reflect micro-scale differences in the symbiosis activity (Nedoncelle et al., 2014-for mussel shell differences), source methane isotopic composition, and/or mussel metabolic function (among tissue differences). Large ranges in $\delta^{13}C$ (BCS, CR values) for mussel tissues may be due to changes in the methane isotopic composition associated with microbial alteration within the sediment, which has also been shown to vary over short distances (Joye et al., 2010). For example, within one collection, BCS $\delta^{13}C$ values ranged from -67.8 to -59.0‰, and for NCS, -66.6 to -59.7‰. Riekenberg et al. (2016) indicated that boundaries or edge effects influenced the “seep” contribution to mussel populations; seep source contributions dominated at the edge of mussel beds rather than in the interior of the beds, which was contrary to expectations. Based on LMM results, we found that larger patches were associated with lower $\delta^{13}C$, $\delta^{15}N$, and higher $\delta^{34}S$, whereas smaller patches generally had

mussels with higher $\delta^{13}C$, $\delta^{15}N$ and lower $\delta^{34}S$ (Fig. 4). Patchiness in resource contribution within a small patch or large bed of mussels suggests that resource availability is variable on the scales of meters to 10s of meters. Findings from our research tested at different seep settings, such as those linked to diapirs (e.g., Blake Ridge) or at seeps where methane is derived from thermogenic processes, would clarify the role of mussel patch size on seep-derived energy use.

The LMM results suggest temporal changes in resource use, with isotopic variance among sampled tissues indicating different turnover times and differences in food sources on a seasonal scale. For transplanted *B. childressi* in the GOM, 100% tissue turnover of carbon, nitrogen, and sulfur isotopes had not occurred after one year, suggesting that mussel tissues integrate their diet over longer time scales (Dattagupta et al., 2004). Based on these slow turnover rates, we propose that tissue measurements at BCS and NCS represent integrated food resources starting with the year prior to collection or even longer. Due to these slow turnover times, we might not expect isotope differences to be evident between the August 2012 and May 2013 mussel collections (within a year) from the same site; however, LMM predicted $\delta^{13}C$ and $\delta^{15}N$ values (Fig. 3, Supplemental Fig. 2) illustrate temporal differences, which may result from changes in the relative utilization of different resources due to seasonally variable inputs and/or temporal and spatial variability in the isotopic values of the food resources (e.g., seasonal phytodetrital input). However, on longer time scales, there does not appear to be large fluctuations in the isotopic value of the methane reservoir given similarities between gill (this study) and periostracum (Prouty et al., 2016a) $\delta^{13}C$ values. In the future, results from our estimates of resource contribution could be evaluated over the organisms' lifespans by employing a similar isotope study to mussel shell periostracum given the similarity between gill and periostracum isotope values.

For a subset of mussels at BCS, $\delta^{15}N$ isotopic differences in mussels were based on mussel size, suggesting ontogenetic changes in nitrogen resource contributions. This relationship may be related to a reliance on phytodetritus relative to chemosymbionts during mussel settlement versus acquisition of endosymbionts after settlement (Laming et al., 2018). Trask and Van Dover (1999) also documented ontogenetic variation in mussel isotope composition, with both $\delta^{13}C$ and $\delta^{15}N$ data positively correlated with mussel size at vents. Similarly, Riekenberg et al. (2016, 2018) observed an ontogenetic shift to lower $\delta^{13}C$ values with increased mussel shell size in GOM mussels. We did not find a correlation between $\delta^{13}C$ and mussel size, which is inconsistent with these previous studies. However, it is possible that the mussels we collected on USAM had already undergone an ontogenetic shift in resource use, from reliance on POM to chemosynthesis (e.g., Laming et al., 2018), but because of the range in mussel sizes that was analyzed, this change was missed. Stable isotope analysis of mussel tissues from a range of size classes would improve our understanding of diet changes with mussel growth.

4.5. Seep food webs

Previous food-web studies at seeps suggest that taxa are found along a gradient of available food resources, with some degree of mixing between chemosynthetic and phytodetrital-derived foods (Levin and Michener, 2002), and that the sphere of influence of seep-derived nutrition can be patchy (Demopoulos et al., 2010; Levin et al., 2016). At BCS and NCS, this influence was variable. In terms of basal sources, bottom water POM was depleted in ^{13}C at both seep sites, possibly due to the contribution of isotopically-light, free-living bacteria present in the bottom water or suspended sediment, consistent with isotopically light microbes ($\delta^{13}C$ = -29.4‰) that were isolated from surface sediments at NCS. Only a few taxa collected from the two seeps

exhibited $\delta^{13}C$ values consistent with reliance on chemosynthetic production. From BCS, fauna utilizing seep production included the sea star *O. robustus* and fishes *D. rugosa* and *S. nebulosus*. While there are no published diet data on *O. robustus*, congeners are considered omnivores, scavengers, and deposit feeders, and generally consume organic matter within the sediment environment (Jangoux and Lawrence 1982). The fishes, *D. rugosa* and *S. nebulosus*, are generally infaunal pickers (Demopoulos et al., 2017), likely consuming sediment fauna depleted in ^{13}C. They were common on complex seep habitats of the shallower Baltimore Canyon site, were intimately associated with benthic seep features (e.g., bubble plumes, live and dead mussel shells), and likely exhibit little movement once on preferred habitats (Ross et al., 2015). Since these fishes occur widely in other non-seep habitats, their utilization of chemosynthetic material seems facultative. In addition, while the average $\delta^{13}C$ value for the polychaete *Hyalinoecia* cf. *tubicola* indicates that these taxa rely on photosynthetically derived material, several individuals were isotopically light (-23.9 and -25.2‰), signifying potential utilization of seep-derived organic matter that is depleted in ^{13}C. However, the measured $\delta^{13}C$ values indicate that most other taxa collected from the BCS environment, from primary consumers to higher-order consumers, relied on photosynthetically derived organic matter, consistent with $\delta^{13}C$ values (-22.2‰) measured from fresh organic matter collected in sediment traps (Prouty et al., 2017; Mienis et al., 2017). The deeper seep environment at NCS also hosted several heterotrophic invertebrate species that utilized chemosynthetic production, including the shrimps (*Alvinocaris markensis*) and urchins (*Echinus wallisi*, *Gracilechinus affinis*). A single specimen of *B. heckerae* was collected at NCS, representing the first occurrence of this species north of Blake Ridge. *Bathymodiolus heckerae* is known to have both thiotrophic and methanotrophic endosymbionts (Cavanaugh et al., 1987; Van Dover et al., 2003), utilizing seawater DIC and

methane as a carbon source. The $\delta^{13}C$ values (-35.1 to -33.7‰) from *B. heckerae* collected from NCS were enriched in ^{13}C compared to previously published isotope values from *B. heckerae* (-55.7‰; Van Dover et al., 2003). This species is known to harbor four phylotypes of symbionts: two thiotrophic, one methanotroph group, and another that groups with the methylotrophs (Becker et al., 2010). Differences in *B. heckerae* and *B. childressi* $\delta^{13}C$ values may be attributed to the relative contribution of dual symbioses (methanotrophs vs. thiotrophs), given that these two mussel species were collected in the same area. Because certain mobile seep-associates found at NCS appear to rely on chemosynthetically-derived nutrition, the contribution of seep energy to the adjacent deep-sea benthos along the USAM may be significant.

5. **Conclusion**

Overall, nutrition at the BCS and NCS is fueled by microbial methane, chemosynthetic bacteria, photosynthetically derived detritus, and suspended POM. The combination of food resources identified in MixSIAR analysis indicates that while USAM *B. childressi* are mixotrophic, their dominant source is methane. Free-living chemoautotrophs on surfaces or in the water column can serve as food for deposit and suspension feeders (Demopoulos et al., 2010). Bacterial mats were extensive in some areas observed on the ROV dives, and they may serve as a significant source of nutrients to the benthos (Levin and Mendoza, 2007). The high diversity of isotopic compositions present at both sites indicates substantial trophic complexity that may result from high microbial diversity (Demopoulos et al., 2010), as well as spatially variable food resources available in different mussel bed habitats (Fig. 4). The presence of these seeps and the variety of food resources available within increase the overall trophic diversity for the canyon and slope environments present in this region. Given that hundreds of seafloor

methane seeps within the region remain to be characterized, primary production present at seeps may serve as an important, yet unrealized, energy source to the USAM deep-sea environment.

Acknowledgements: We thank the ship and shore-based personnel and all the science and outreach personnel for their hard work during the cruises. We thank the captain and crew of the R/Vs Hugh Sharp and Atlantis, and NOAA ships Ron Brown and Nancy Foster, and the submersible groups supporting Jason and Alvin (WHOI), Kraken (UCONN), and Global Explorer (Oceaneering). This study was conducted by the Ecosystems Mission Area of USGS to meet information needs identified by the Bureau of Ocean Energy Management and funding was provided to AWJD by the USGS Environments program. N.P. and C.R. were supported by the USGS Coastal and Marine program, and additional funding to A.D., N.P., and CR was provided under USGS-NOAA interagency agreement 16-01118. S.B. and S.W.R. were funded by the Bureau of Ocean Energy Management (BOEM) through a contract from CSA Ocean Sciences, Inc. (contract M10PC00100). NOAA ships, ROVs, and data management support were provided by the NOAA OER. Thanks to G. Boland (BOEM), C. Charles, and M. Anderson, L. Ball, and M. Khalil (USGS) for their continued support. A special thank you to C. Van Dover for facilitating sediment collections on her SeepC cruise in 2015. Thanks to F. Mienis, M. Lavaleye, G. Duineveld, and M. Rhode for their assistance at sea, to R. Lee, WSU, for isotope analyses, and to J. Pohlman (USGS) for access to some $\delta^{13}C$ analyses for methane. We are particularly grateful to C. Mah, C. Robertson, and other taxonomic experts that assisted with this complex study. Any use of trade, product, or firm names is for descriptive purposes only and does not imply endorsement by the US Government.

References:

Assie, A., Borowski, C., van der Heijden, K., Raggi, L., Geier, B., Leisch, N., . . . Petersen, J. M. (2016). A specific and widespread association between deep-sea Bathymodiolus mussels and a novel family of Epsilonproteobacteria. *Environmental Microbiology Reports, 8*(5), 805-813. doi:10.1111/1758-2229.12442

Barnes, C., Jennings, S., Polunin, N.V.C., Lancaster, J.E., 2008. The importance of quantifying inherent variability when interpreting stable isotope field data. Oecologia 155 (2), 227-235.

Becker, E.L., Cordes, E.E., Macko, S.A., Lee, R.W., Fisher, C.R., 2014. Spatial patterns of tissue stable isotope contents give insight into the nutritional sources for seep communities on the Gulf of Mexico lower slope. Marine Ecology Progress Series 498, 133-145.

Becker, E.L., Lee, R.W., Macko, S.A., Faure, B.M., Fisher, C.R., 2010. Stable carbon and nitrogen isotope compositions of hydrocarbon-seep bivalves on the Gulf of Mexico lower continental slope. Deep Sea Research Part II: Topical Studies in Oceanography 57 (21–23), 1957-1964.

Bourque, J.R., Robertson, C.M., Brooke, S., Demopoulos, A.W.J., 2017. Macrofaunal communities associated with chemosynthetic habitats from the U.S. Atlantic margin: A comparison among depth and habitat types. Deep Sea Research Part II: Topical Studies in Oceanography 137 (42-55).

Brooks, J.M., Kennicutt, M.C., Fisher, C.R., Macko, S.A., Cole, K., Childress, J.J., Bidigare, R.R., Vetter, R.D., 1987. Deep-sea hydrocarbon seep communities: Evidence for energy and nutritional carbon sources. Science 238 (4830), 1138-1142.

Canfield, D., 2001. Biogeochemistry of sulfur isotopes. Reviews in Mineralogy and Geochemistry 43 (1), 607-636.

Cavanaugh, C.M., Levering, P.R., Maki, J.S., Mitchell, R., Lidstrom, M.E., 1987. Symbiosis of methylotrophic bacteria and deep-sea mussels. Nature 325, 346-348.

Chambers, L.A., Trudinger, P.A., 1979. Microbiological fractionation of stable sulfur isotopes: A review and critique. Geomicrobiology Journal 1 (3), 249-293.

Childress, J.J., Fisher, C.R., Brooks, J.M., Kennicutt, M., Bidigare, R., Anderson, A.E., 1986. A methanotrophic marine molluscan (Bivalvia, Mytilidae) symbiosis: Mussels fueled by gas. Science 233 (4770), 1306-1308.

Coykendall, D.K., R.S. Cornman, N.G. Prouty, S. Brooke, A.W.J. Demopoulos, C.L. Morrison, 2019. Molecular characterization of *Bathymodiolus* mussels and gill symbionts associated with chemosynthetic habitats from the U.S. Atlantic margin, in press, Plos One.

CSA Ocean Sciences Inc, Ross, S.W., Brooke, S., Baird, E., Coykendall, D.K., Davies, A.J., Demopoulos, A.W.J., France, S.C., Kellogg, C.A., Mather, R., Mienis, F., Morrison, C., Prouty, N., Roark, B., Robertson, C.M., 2017. Exploration and Research of Mid-Atlantic Deepwater hard Bottom Habitats and Shipwrecks with Emphasis on Canyons and Coral Communities: Atlantic Deepwater Canyons Study. Vol I. Final Technical Rept., Vol. II: Final Appendices., OCS Study BOEM 2017-060 (Vol. I) & 061 (Vol. II). U.S. Dept. of the Interior, Bureau of Ocean Energy Management, Atlantic OCS Region, p. 1000 p + appendices.

Dattagupta, S., Bergquist, D.C., Szalai, E.B., Macko, S.A., Fisher, C.R., 2004. Tissue carbon, nitrogen, and sulfur stable isotope turnover in transplanted *Bathymodiolus childressi* mussels: Relation to growth and physiological condition. *Limnology and Oceanography* 49 (4), 1144-1151.

Demopoulos, A.W.J., Bourque, J.R., Brooke, S., Ross, S.W., 2014. Community structure at newly investigated hydrocarbon seeps on the continential slope of the western north Atlantic. 2014 Ocean Sciences Meeting, Honolulu, HI.

Demopoulos, A.W.J., Gualtieri, D., Kovacs, K., 2010. Food-web structure of seep sediment macrobenthos from the Gulf of Mexico. *Deep Sea Research Part II: Topical Studies in Oceanography* 57 (21–23), 1972-1981.

Demopoulos, A.W.J., McClain-Counts, J., Ross, S.W., Brooke, S., Mienis, F., 2017. Food-web dynamics and isotopic niches in deep-sea communities residing in a submarine canyon and on the adjacent open slopes. *Marine Ecology Progress Series* 578, 19-33.

Demopoulos, A.W.J., Bourque, J.R., Durkin, A., Cordes, E.E., 2018. The influence of seep habitats on sediment macrofaunal biodiversity and functional traits. *Deep Sea Research Part I*, 42 (77-93).

Deuder, S., Cabanellas, M., Blanco, A., Tejada, S. 2009. Stable isotope fractionation in the digestive gland, muscle and gills tissues of the marine mussel Mytilus galloprovincialis. Journal of Experimental Marine Biology and Ecology, 368: 181–188.

Duperron, S., Lorion, J., Samadi, S., Gros, O., & Gaill, F. (2009). Symbioses between deep-sea mussels (Mytilidae: Bathymodiolinae) and chemosynthetic bacteria: diversity, function and evolution. *Comptes Rendus Biologies, 332*(2-3), 298-310. doi:10.1016/j.crvi.2008.08.003

Duperron, S., Sibuet, M., MacGregor, B. J., Kuypers, M. M. M., Fisher, C. R., & Dubilier, N. (2007). Diversity, relative abundance and metabolic potential of bacterial endosymbionts in three Bathymodiolus mussel species from cold seeps in the Gulf of Mexico. *Environmental Microbiology, 9*(6), 1423-1438. doi:10.1111/j.1462-2920.2007.01259.x

Duperron, S., Gaudron, S. M., Rodrigues, C. F., Cunha, M. R., Decker, C., & Olu, K. (2013). An overview of chemosynthetic symbioses in bivalves from the North Atlantic and Mediterranean Sea. *Biogeosciences, 10*(5), 3241-3267. doi:10.5194/bg-10-3241-2013

Duperron, S., Guezi, H., Gaudron, S. M., Ristova, P. P., Wenzhofer, F., & Boetius, A. (2011). Relative abundances of methane- and sulphur-oxidising symbionts in the gills of a cold seep mussel and link to their potential energy sources. *Geobiology, 9*(6), 481-491. doi:10.1111/j.1472-4669.2011.00300.x

Feng, D., Cheng, M., Kiel, S., Qiu, J.W., Yang, Q.H., Zhou, H.Y., Peng, Y.B., Chen, D.F., 2015. Using *Bathymodiolus* tissue stable carbon, nitrogen and sulfur isotopes to infer biogeochemical process at a cold seep in the South China Sea. Deep-Sea Research Part I-Oceanographic Research Papers 104, 52-59.

Fry, B., 2007. Coupled N, C and S stable isotope measurements using a dual-column gas chromatography system. Rapid Communications in Mass Spectrometry 21, 750-756.

Fry, B., Sherr, E.B., 1984. $\delta^{13}C$ measurements as indicators of carbon flow in marine and freshwater ecosystems. Contrib. in Mar. Sci. 27, 13-47.

Fry, B., Gest, H., Hayes, J.M., 1983. Sulfur isotopic composition of deep-sea hydrothermal vent animals. Nature, Lond., 306: 51-52.

Habicht, K.S., Canfield, D.E., Rethmeier, J.o., 1998. Sulfur isotope fractionation during bacterial reduction and disproportionation of thiosulfate and sulfite. Geochimica et Cosmochimica Acta 62 (15), 2585-2595.

Heyl, T.P., Gilhooly, W.P., Chambers, R.M., Gilchrist, G.W., Macko, S.A., Ruppel, C.D., Van Dover, C.L., 2007. Characteristics of vesicomyid clams and their environment at the Blake Ridge cold seep, South Carolina, USA. Marine Ecology Progress Series 339, 169-184.

Jackson, A.L., Inger, R., Parnell, A.C., Bearhop, S., 2011. Comparing isotopic niche widths among and within communities: SIBER - Stable Isotope Bayesian Ellipses in R. Journal of Animal Ecology 80 (3), 595-602.

Jangoux M. and J.M Lawrence (eds). 1982. *Echinoderm nutrition*. Balkema, Rotterdam, 654 p.

Joye, S.B., Bowles, M.W., Samarkin, V.A., Hunter, K.S., Niemann, H., 2010. Biogeochemical signatures and microbial activity of different cold-seep habitats along the Gulf of Mexico deep slope. Deep Sea Research Part II: Topical Studies in Oceanography 57 (21–23), 1990-2001.

Kellermann, M.Y., Schubotz, F., Elvert, M., Lipp, J.S., Birgel, D., Prieto-Mollar, X., Dubilier, N., Hinrichs, K.U., 2012. Symbiont-host relationships in chemosynthetic mussels: A comprehensive lipid biomarker study. Organic Geochemistry 43, 112-124.

Laming, S.R., Gaudron, S.M., Duperron, S., 2018. Lifecycle ecology of deep-sea chemosymbiotic mussels: a review. Frontiers in Marine Science 5, 282

Layman, C.A., Arrington, D.A., Montana, C.G., Post, D.M., 2007. Can stable isotope ratios provide for community-wide measures f trophic structure? Ecology 88 (1), 42-48.

Lee, R.W., Childress, J.J., 1996. Inorganic N assimilation and ammonium pools in a deep-sea mussel containing methanotrophic endosymbionts. Biological Bulletin 190 (3), 373-384.

Lee, R.W., Thuesen, E.V., Childress, J.J., Fisher, C.R., 1992. Ammonium and free amino-acid-uptake by a deep-Sea mussel (*Bathymodiolus* sp., Undescribed) containing methanotrophic bacterial symbionts. Marine Biology 113 (1), 99-106.

Levin, L.A., 2005. Ecology of cold seep sediments: interactions of fauna with flow, chemistry and microbes. Oceanography and Marine Biology: An Annual Review 43, 1-46.

Levin, L.A., Baco, A.R., Bowden, D., Colaço, A., Cordes, E., Cunha, M.R., Demopoulos, A., Gobin, J., Grupe, B., Le, J., Metaxas, A., Netburn, A., Rouse, G.W., Thurber, A.R., Tunnicliffe, V., Van Dover, C., Vanreusel, A., Watling, L., 2016. Hydrothermal vents and methane seeps: rethinking the sphere of influence. Frontiers in Marine Science 3.

Levin, L.A., Mendoza, G.F., 2007. Community structure and nutrition of deep methane-seep macrobenthos from the North Pacific (Aleutian) margin and the Gulf of Mexico (Florida Escarpment). Marine Ecology 28, 131-151.

Levin, L.A., Michener, R.H., 2002. Isotopic evidence for chemosynthesis-based nutrition of macrobenthos: the lightness of being at Pacific methane seeps. Limnol. Oceanogr. 47 (5), 1336-1345.

McVeigh, D., Skarke, A., Dekas, A.E., Borrelli, C., Hong, W.L., Marlow, J.J., Pasulka, A., Jungbluth, S.P., Barco, R.A., Djurhuus, A., 2018. Characterization of benthic biogeochemistry and ecology at three methane seep sites on the Northern U.S. Atlantic margin. Deep Sea Research Part II: Topical Studies in Oceanography 150, 41-56.

Mienis, F., Duineveld, G.C.A., Roark, B., Demopoulos, A.W.J., Prouty, N., Campbell-Swarzenski, P., Rhode, M., Brooke, S., Ross, S.W., 2017. Chapter 6: Geological Studies. In: CSA Ocean Sciences Inc., S. Ross, S. Brooke, E. Baird, E. Coykendall, A. Davies, A. Demopoulos, S. France, C. Kellogg, R. Mather, F. Mienis, C. Morrison, N. Prouty, B. Roark and C. Robertson. 2017. In: Exploration and Research of Mid-Atlantic Deepwater hard Bottom Habitats and Shipwrecks with Emphasis on Canyons and Coral Communities: Atlantic Deepwater Canyons Study. Vol I. Final Technical Rept., Vol. II: Final Appendices. U.S. Dept. of the Interior, Bureau of Ocean Energy Management, Atlantic OCS Region. OCS Study BOEM 2017-060 (Vol. I) & 061 (Vol. II), pp. 211-262.

Nedoncelle, K., Le Bris, N., de Rafelis, M., Labourdette, N., Lartaud, F., 2014. Non-equilibrium fractionation of stable carbon isotopes in chemosynthetic mussels. Chemical Geology 387, 35-46.

Page, H.M., Fisher, C.R., Childress, J.J., 1990. Role of filter-feeding in the nutritional biology of a deep-sea mussel with methanotrophic symbionts. Marine Biology 104 (2), 251-257.

Page, H. M., Fialamedioni, A., Fisher, C. R., & Childress, J. J. (1991). Experimental-Evidence for Filter-Feeding by the Hydrothermal Vent Mussel, Bathymodiolus-Thermophilus. *Deep-Sea Research Part A-Oceanographic Research Papers, 38*(12), 1455-1461. doi:Doi 10.1016/0198-0149(91)90084-S

Paull, C., Lorenson, T., Borowski, W., Ussler III, W., Olsen, K., Rodriguez, N., 2000. Isotopic composition of CH4, CO2 species, and sedimentary organic matter within samples from the Blake Ridge: Gas source implications. Proceedings of the Ocean Drilling Program, Scientific Results. Citeseer, pp. 67-78.

Paull, C.K., Ussler, W., Borowski, W.S., Spiess, F.N., 1995. Methane-rich plumes on the Carolina continental rise: Associations with gas hydrates. Geology 23 (1), 89-92.

Phillips, D.L., Inger, R., Bearhop, S., Jackson, A.L., Moore, J.W., Parnell, A.C., Semmens, B.X., Ward, E.J., 2014. Best practices for use of stable isotope mixing models in food-web studies. Canadian journal of zoology 92 (10), 823-835.

Pile, A.J., Young, C.M., 1999. Plankton availability and retention efficiencies of cold-seep symbiotic mussels. Limnology and Oceanography 44 (7), 1833-1839.

Pinnegar, J.K., Polunin, N.V.C., 1999. Differential fractionation of $\delta^{13}C$ and $\delta^{15}N$ among fish tissues: implications for the study of trophic interactions. Functional Ecology 13 (2), 225-231.

Pohlman, J., Ruppel, C., Colwell, F., Krause, S., Treude, T., Graw, M., Casso, M., Boze, L., Buczkowski, B., Brankovits, D., 2015. Sediment and water column geochemistry related to methane seepage along the northern US Atlantic margin. American Geophysical Union, Fall Meeting 2015, San Diego, CA, OS11B-0702.

Pohlman, J.W., Ruppel, C.D., Wang, D.T., Ono, S., Kluesner, J., Xu, X., Sylva, S., Casso, M., 2017. Natural gas sources from methane seeps on the Northern U.S. Atlantic Margin. American Geophysical Union, Fall Meeting 2017, New Orleans, LA, OS33A-1992.

Post, D.M., Layman, C.A., Arrington, D.A., Takimoto, G., Quattrochi, J., Montana, C.G., 2007. Getting to the fat of the matter: models, methods and assumptions for dealing with lipids in stable isotope analyses. Oecologia 152, 179-189.

Prouty, N.G., Mienis, F., Campbell-Swarzenski, P., Roark, E.B., Davies, A.J., Robertson, C.M., Duineveld, G., Ross, S.W., Rhode, M., Demopoulos, A.W.J., 2017. Seasonal variability in the source and composition of particulate matter in the depositional zone of Baltimore Canyon, U.S. Mid-Atlantic Bight. Deep Sea Research Part I: Oceanographic Research Papers 127 (Supplement C), 77-89.

Prouty, N.G., Sahy, D., Ruppel, C.D., Roark, E.B., Condon, D., Brooke, S., Ross, S.W., Demopoulos, A.W.J., 2016a. Insights into methane dynamics from analysis of authigenic carbonates and chemosynthetic mussels at newly-discovered Atlantic Margin seeps. Earth and Planetary Science Letters 449, 332-344.

Prouty, N.G, Sahy, D., Condon, D., Roark, E.B., Ruppel, C. and Demopoulos, A.W.J. 2016b. Geochemical analysis of authigenic carbonates and chemosynthetic mussels. USGS Data Release, DOI: 10.5066/F77942SJ

Pruski, A.M., Fiala-Medioni, A., Fisher, C.R., Colomines, J.C., 2000. Composition of free amino acids and related compounds in invertebrates with symbiotic bacteria at hydrocarbon seeps in the Gulf of Mexico. Marine Biology 136 (3), 411-420.

Quattrini, A.M., Nizinski, M.S., Chaytor, J.D., Demopoulos, A.W.J., Roark, E.B., France, S.C., Moore, J.A., Heyl, T., Auster, P.J., Kinlan, B., Ruppel, C., Elliott, K.P., Kennedy, B.R.C., Lobecker, E., Skarke, A., Shank, T.M., 2015. Exploration of the canyon-incised continental margin of the northeastern United States reveals dynamic habitats and diverse communities. PloS one 10 (10).

R Development Core Team, 2018. R: A language and environment for statistical computing. . R Foundation for Statistical Computing Vienna, Austria.

Reid, W.D.K., Sweeting, C.J., Wigham, B.D., McGill, R.A.R., Polunin, N.V.C., 2016. Isotopic niche variability in macroconsumers of the East Scotia Ridge (Southern Ocean) hydrothermal vents: What more can we learn from an ellipse? Marine Ecology Progress Series 542, 13-24.

Riekenberg, P.M., Carney, R.S., Fry, B., 2016. Trophic plasticity of the methanotrophic mussel *Bathymodiolus childressi* in the Gulf of Mexico. Marine Ecology Progress Series 547, 91-106.

Riekenberg, P. M., Carney, R. S., & Fry, B. (2018). Shell carbon isotope indicators of metabolic activity in the deep-sea mussel Bathymodiolus childressi. *Deep-Sea Research Part I-Oceanographic Research Papers, 134*, 48-54. doi:10.1016/j.dsr.2018.02.004

Riou, V., Duperron, S., Halary, S., Dehairs, F., Bouillon, S., Martins, I., Colaco, A., Santos, R.S., 2010a. Variation in physiological indicators in *Bathymodiolus azoricus* (Bivalvia: Mytilidae) at the Menez Gwen Mid-Atlantic Ridge deep-sea hydrothermal vent site within a year. Marine Environmental Research 70 (3-4), 264-271.

Riou, V., Colaco, A., Bouillon, S., Khripounoff, A., Dando, P., Mangion, P., Chevalier, E., Korntheuer, M., Santos, R.S., Dehairs, F. (2010b). Mixotrophy in the deep sea: a dual endosymbiotic hydrothermal mytilid assimilates dissolved and particulate organic matter. *Marine Ecology Progress Series, 405*, 187-201. doi:10.3354/meps08515

Rodrigues, C.F., Hilario, A., Cunha, M.R., 2013. Chemosymbiotic species from the Gulf of Cadiz (NE Atlantic): distribution, life styles and nutritional patterns. Biogeosciences 10 (4), 2569-2581.

Romanek, C.S., Grossman, E.L., Morse, J.W., 1992. Carbon isotopic fractionation in synthetic aragonite and calcite: Effects of temperature and precipitation rate. Geochimica et Cosmochimica Acta 56 (1), 419-430.

Ross, S.W., Rhode, M., Quattrini, A.M., 2015. Demersal fish distribution and habitat use within and near Baltimore and Norfolk Canyons, U.S. middle Atlantic slope. Deep Sea Research Part I: Oceanographic Research Papers 103, 137-154.

Ruppel, C., Demopoulos, A., Prouty, N., Sahy, D., Condon, D., 2017, Exploring U.S. Atlantic margin seeps with a remotely-operated vehicle, U.S. Department of Energy National Energy Technology Laboratory's Fire in the Ice 17(2), 12-15.

Skarke, A., Ruppel, C., Kodis, M., Brothers, D., Lobecker, E., 2014. Widespread methane leakage from the sea floor on the northern US Atlantic margin. Nature Geoscience 7 (9), 657-661.

Stock, B. C. and Semmens, B.X. 2016. MixSIAR GUI User Manual. Version 3.1. https://github.com/brianstock/MixSIAR/. doi:10.5281/zenodo.47719.

Streams, M.E., Fisher, C.R., FialaMedioni, A., 1997. Methanotrophic symbiont location and fate of carbon incorporated from methane in a hydrocarbon seep mussel. Marine Biology 129 (3), 465-476.

Thurber, A.R., Kroeger, K., Neira, C., Wiklund, H., Levin, L.A., 2010. Stable isotope signatures and methane use by New Zealand cold seep benthos. Marine Geology 272 (1-4), 260-269.

Trask, J.L., Van Dover, C.L., 1999. Site-specific and ontogenetic variations in nutrition of mussels (*Bathymodiolus* sp.) from the Lucky Strike hydrothermal vent field, Mid-Atlantic Ridge. Limnology and Oceanography 44 (2), 334-343.

Van Dover, C.L., 2000. The ecology of hydrothermal vents. Princeton University Press, Princeton, NJ.

Van Dover, C.L., 2007. Stable isotope studies in marine chemoautotrophically based ecosystems: An update. In: Michener, R., Lajtha, K. (Eds.), Stable isotopes in ecology and environmental sciences. Blackwell Publishing, Second Edition, pp. 202-237.

Van Dover, C.L., Aharon, P., Bernhard, J.M., Caylor, E., Doerries, M., Flickinger, W., Gilhooly, W., Goffredi, S.K., Knick, K.E., Macko, S.A., Rapoport, S., Raulfs, E.C., Ruppel, C., Salerno, J.L., Seitz, R.D., Sen Gupta, B.K., Shank, T., Turnipseed, M., Vrijenhoek, R., 2003. Blake Ridge methane seeps: characterization of a soft-sediment, chemo synthetically based ecosystem. Deep-Sea Research Part I-Oceanographic Research Papers 50 (2), 281-300.

Vetter, R.D., Fry, B., 1998. Sulfur contents and sulfur-isotope compositions of thiotrophic symbioses in bivalve molluscs and vestimentiferan worms. Marine Biology 132 (3), 453-460.

Yamanaka, T., Mizota, C., Satake, H., Kouzuma, F., Gamo, T., Tsunogai, U., Miwa, T., Fujioka, K., 2003. Stable isotope evidence for a putative endosymbiont-based lithotrophic *Bathymodiolus* sp. mussel community atop a serpentine seamount. Geomicrobiology Journal 20 (3), 185-197.

Yamanaka, T., Shimanura, S., Nagashio, H., Yamagami, S., Onishi, Y., Hyodo, A., Mampuku, M., Mizota, C., 2015. A compilation of the stable isotopic compositions of carbon, nitrogen, and sulfur in soft body parts of animals collected from deep-sea hydrothermal vent and methane seep fields: variations in energy source and importance of subsurface microbial processes in the sediment-hosted systems. In: Ishibashi, J.-I., Okino, K., Sunamura, M. (Eds.), Subseafloor Biosphere Linked to Hydrothermal Systems. Springer, pp. 105–129.

Table 1. Average $\delta^{13}C$, $\delta^{15}N$, and $\delta^{34}S$ (‰ ± SD) and C:N ratio for different tissue types sampled from the mussels *Bathymodiolus childressi* collected in seeps located near Baltimore (BCS) and Norfolk (NCS) canyons. Values in parentheses represent the range. Values in brackets next to n value indicated the number of samples analyzed for sulfur isotopes.

	BCS					NCS				
Tissue	n	$\delta^{13}C$	$\delta^{15}N$	$\delta^{34}S$	C:N	n	$\delta^{13}C$	$\delta^{15}N$	$\delta^{34}S$	C:N
Gill	54 [10]	-63.0 ± 1.9	0.2 ± 1.1	12.6 ± 4.9	5.1 ± 0.6	87 [11]	-62.9 ± 2.2	0.6 ± 1.2	14.0 ± 2.7	5.2 ± 0.4
		(-67.8 to -59.0)	(-1.6 to 3.0)	(0.1 to 18.5)	(3.4 to 6.7)		(-71.2 to -59.5)	(-2.2 to 3.5)	(10.6 to 18.7)	(4.2 to 6.3)
Mantle	52 [10]	-64.6 ± 2.6	0.8 ± 1.3	12.1 ± 2.4	6.4 ± 1.6	86 [13]	-62.8 ± 3.0	1.7 ± 1.1	15.1 ± 2.9	5.7 ± 1.3
		(-73.6 to -59.3)	(-1.6 to 6.3)	(6.3 to 15.6)	(4.1 to 9.4)		(-69.8 to -54.4)	(-0.9 to 4.5)	(8.7 to 19.7)	(3.9 to 9.3)
Muscle	54 [10]	-61.7 ± 2.1	1.3 ± 1.2	11.0 ± 6.2	4.0 ± 0.6	37 [10]	-60.8 ± 2.0	2.5 ± 1.0	15.3 ± 2.9	4.1 ± 0.2
		(-68.4 to -58.5)	(-1.3 to 4.3)	(-4.1 to 17.0)	(3.2 to 6.2)		(-65.6 to -57.8)	(-0.1 to 4.5)	(11.0 to 19.9)	(3.6 to 4.9)

Table 2. Average $\delta^{13}C$ and $\delta^{15}N$ (‰ ± SD) and C:N ratio for fishes, invertebrates (excluding *Bathymodiolus childressi*), sediments and producers collected in seeps located near Baltimore (BCS) and Norfolk (NCS) canyons. A $\delta^{34}S$ value is reported for the one specimen of *Bathymodiolus heckerae*. Values in parentheses represent the min-max range. Feeding groups (G) are defined as deposit (d), benthic (b), pelagic (p), mix of benthic and pelagic (b/p), chemosynthetic (c), infauna (i), suprabenthic (sb), suspension (s) and unknown (u).

		BCS				NCS				
Taxa	G	N	$\delta^{13}C$	$\delta^{15}N$	C:N	N	$\delta^{13}C$	$\delta^{15}N$	$\delta^{34}S$	C:N
Annelida										
Eunicicae										
Hyalinoecia artifex	d	11	-17.8 ± 0.2	9.1 ± 1.1	4.1 ± 0.3					
			(-18.2 to -17.5)	(7.2 to 10.6)	(3.7 to 4.8)					
Hyalinoecia tubicola	d	12	-19.2 ± 1.8	10.0 ± 0.6	4.4 ± 0.4					
			(-23.8 to -17.2)	(9.2 to 11.2)	(4.0 to 5.4)					
Arthropoda										
Amphipoda										
Amphipoda	b/p	16	-19.4 ± 0.9	6.1 ± 0.5	4.3 ± 0.6					
			(-21.3 to -18.1)	(5.1 to 6.8)	(3.1 to 5.3)					
Lestrigonidae										
cf. Hyperietta luzoni	b/p	16	-18.7 ± 0.6	7.0 ± 0.8	4.6 ± 0.2					
			(-19.6 to -17.6)	(6.0 to 8.8)	(4.2 to 5.1)					
Hyperiidae										
Themisto sp.	p	11	-18.9 ± 0.6	6.9 ± 1.2	4.4 ± 0.7					
			(-19.8 to -17.5)	(3.8 to 8.1)	(2.5 to 5.0)					
Decapoda										
Alvinocarididae										
Alvinocaris markensis	c					7	-51.2 ± 4.6	5.2 ± 0.6		3.7 ± 0.2
							(-60.4 to -46.7)	(4.2 to 5.8)		(3.5 to 4.0)
Chirostylidae										
Eumunida picta	b	3	-20.0 ± 1.4	9.8 ± 0.4	4.2 ± 0.1					

			(-21.6 to -18.8)	(9.4 to 10.2)	(4.0 to 4.3)
Munididae					
Munida valida	b	2	-18.5 ± 0.9	8.7 ± 0.1	4.0 ± 0.3
			(-19.1 to -17.9)	(8.7 to 8.8)	(3.7 to 4.2)
Diogenidae					
Paguristes cf. moorei	b	3	-21.9 ± 2.3	10.3 ± 0.3	4.2 ± 0.1
			(-23.5 to -19.2)	(10.0 to 10.7)	(4.1 to 4.3)
Paguristes lymani	b	3	-18.4 ± 0.9	10.5 ± 0.9	3.7 ± 0.7
			(-19.0 to -17.4)	(9.7 to 11.5)	(2.8 to 4.1)
Pandalidae					
Pandalus montagui	sb	1	-18.6	9.8	3.6
Shrimp sp.	u	9	-19.1 ± 0.7	6.2 ± 0.9	3.9 ± 0.3
			(-19.8 to -17.3)	(4.8 to 7.3)	(3.5 to 4.6)
Euphausiacea	u	1	-19.1	7.6	5.0
Euphausiidae					
Euphausiidae	p	4	-19.1 ± 0.2	7.1 ± 0.5	4.7 ± 0.4
			(-19.3 to -18.8)	(6.6 to 7.8)	(4.2 to 5.1)
Nyctiphanes couchii	p	4	-19.1 ± 0.4	6.7 ± 0.6	4.1 ± 0.1
			(-19.6 to -18.8)	(6.0 to 7.4)	(4.0 to 4.2)
cf. Thysanoessa macrura	p	10	-19.3 ± 0.6	7.6 ± 0.9	4.1 ± 0.2
			(-20.5 to -18.2)	(5.9 to 8.8)	(3.8 to 4.5)
Thysanoessa macrura	p	8	-18.9 ± 0.3	8.0 ± 0.6	4.1 ± 0.2
			(-19.2 to -18.5)	(7.0 to 8.9)	(3.8 to 4.3)
Chordata - Fish					
Anguilliformes					
Synaphobranchidae					
Dysommina rugosa	b	7	-30.0 ± 9.4	8.4 ± 2.0	4.4 ± 0.3
			(-48.1 to -20.2)	(5.2 to 10.9)	(4.2 to 5.1)

Aulopiformes					
Paralepididae					
Arctozenus risso	p	3	-19.0 ± 0.7	8.6 ± 0.3	4.6 ± 0.3
			(-19.6 to -18.3)	(8.3 to 8.9)	(4.2 to 4.8)
Myctophiformes					
Myctophidae					
Ceratoscopelus maderensis	p	3	-18.7 ± 0.1	9.2 ± 0.3	4.6 ± 0.1
			(-18.9 to -18.6)	(8.9 to 9.5)	(4.5 to 4.7)
Pleuronectiformes					
Cynoglossidae					
Symphurus nebulosus	i	4	-24.5 ± 1.4	10.4 ± 0.4	4.1 ± 0.1
			(-25.5 to -22.5)	(10.0 to 10.9)	(4.0 to 4.1)
Cnidaria					
Alcyonacea					
Paragorgiidae					
Paragorgia arborea	s	3	-22.0 ± 0.7	3.8 ± 1.7	4.2 ± 0.6
			(-22.7 to -21.5)	(1.9 to 4.9)	(3.6 to 4.6)
Zoantharia					
Zoantharia sp.	s	1	-22.3	6.9	5.4
Echinodermata					
Ophiurida					
Ophiuridae					
Ophiopholis aculeata	d	1	-23.9	6.4	3.1
Valvatida					
Odontasteridae					
Odontaster robustus	b	3	-44.0 ± 2.0	6.2 ± 1.9	2.6 ± 0.4
			(-46.1 to -42.0)	(4.0 to 7.7)	(2.1 to 3.0)

Echinoida										
Echinidae										
Echinus wallisi	d					9	-57.0 ± 2.0	2.5 ± 0.8		5.3 ± 0.4
							(-59.8 to -52.5)	(1.1 to 3.6)		(4.6 to 6.0)
Gracilechinus affinis	d					11	-55.7 ± 3.6	3.7 ± 1.5		6.1 ± 0.7
							(-58.7 to -47.1)	(1.7 to 6.8)		(5.0 to 7.7)
Mollusca										
Mytiloida										
Mytilidae										
Bathymodiolus heckerae (gill)	c					1	-34.3	1.8	1.4	5.1
Bathymodiolus heckerae (mantle)	c					1	-35.1	3.1	4.6	6.0
Bathymodiolus heckerae (muscle)	c					1	-33.7	3.5	3.3	4.2
Oegopsida										
Ommastrephidae										
Illex cf. *illecebrosus*	p	2	-20.6 ± 1.1	9.6 ± 0.9	4.3 ± 0.1					
			(-21.4 to -19.9)	(9.0 to 10.3)	(4.3 to 4.4)					
Other										
Microbial mat						1	-29.4	7.3		5.3
POM (bottom)		4*	-24.7 ± 2.2	6.1 ± 3.3		4*	-24.7 ± 3.3	3.0 ± 1.4		
			(-27.7 to -22.9)	(1.5 to 8.6)			(-28.9 to -21.5)	(2.0 to 4.9)		
POM (midwater)		3	-21.8 ± 1.2	5.0 ± 1.2						
			(-22.8 to -20.4)	(4.1 to 6.3)						
POM (surface)						2	-21.6 ± 1.6	3.5 ± 0.1		
							(-22.7 to -20.5)	(3.4 to 3.5)		
Sediment (0-2cm)		4	-23.4 ± 2.9	4.8 ± 0.3		5	-30.7 ± 8.2	4.8 ± 1.7		
			(-27.1 to -20.1)	(4.3 to 5.1)			(-40.3 to -24.0)	(2.8 to 6.7)		

*For POM (bottom) samples, n=4 for $\delta^{13}C$ data and n=3 for $\delta^{15}N$ and C:N data.

Table 3. Isotope niche area (‰^{2}) estimates (sample size-corrected standard ellipse area, SEA_C; and Bayesian SEA, SEA_B), including 95% credible intervals calculated from the isotopic values from different mussel tissues found in BCS and NCS. Bold values were significantly higher ($p<0.05$) than other tissues within the same site (e.g., BCS mantle vs. muscle), underlined values represent significant differences between sites for the same tissue pairs.

	N	SEAc	SEA_B	95% CI	
BCS					
Gill	54	6.13	<u>5.95</u>	4.51	7.84
Mantle	52	10.72	**10.36**	7.79	13.74
Muscle	54	8.00	7.81	5.89	10.19
NCS					
Gill	87	8.11	<u>7.93</u>	6.46	9.83
Mantle	86	10.67	**10.40**	8.54	12.88
Muscle	37	6.28	6.03	4.23	8.28

Table 4. Mean probability values of Layman metrics for BCS and NCS mussel populations. Values in bold were significantly higher ($p< 0.01$) than corresponding seep pair.
NR: $\delta^{15}N$ range; CR: $\delta^{13}C$ range, CD: distance to centroid; NND: nearest neighbor distance; SDNND: standard deviation of nearest neighbor distance.

	BCS	95% CI	NCS	95% CI
NR	1.10	0.71 to 1.48	**1.87**	1.49 to 2.27
CR	**2.89**	2.50 to 3.27	2.01	1.66 to 2.42
CD	1.19	1.04 to 1.34	1.14	0.99 to 1.30
NND	**1.70**	1.43 to 1.91	1.39	1.18 to 1.62
SDNND	0.00	-0.01 to 0.35	**0.63**	0.33 to 0.94

Table 5. Isotopic endmembers (mean, standard deviation) used in the MixSIAR model to estimate proportional contributions to mussel populations. Values are based on published data and results presented in this study.

		$\delta^{13}C$ (‰)		$\delta^{15}N$ (‰)		$\delta^{34}S$ (‰)		
Sources	n	Mean	SD	Mean	SD	Mean	SD	References:
Phytodetritus	5	-22.3	0.2	5.0	0.1	20.5	0.2	$\delta^{13}C$, $\delta^{15}N$: This study, $\delta^{34}S$: Heyl et al., 2007
Thiotrophic microbes	4	-32.8	1.8	-3.5	2.0	-6.6	1.4	$\delta^{13}C$, $\delta^{15}N$: Demopoulos et al., 2010, $\delta^{34}S$: Heyl et al., 2007
Seep-1	4	-100.4	7.6	-3.5	2.0	20.5	0.2	$\delta^{13}C$: Pohlman, 2018, $\delta^{15}N$: Demopoulos et al., 2010, $\delta^{34}S$: Heyl et al., 2007
Seep-2	3	-67.6	2.3	4.8	1.2	-6.6	1.4	$\delta^{13}C$: Paull et al., 1995, Pohlman, 2015, $\delta^{15}N$: this study, $\delta^{34}S$: Heyl et al., 2007

Figure 1. Map of the U.S. Mid-Atlantic margin with red boxes indicating the location of the Baltimore and Norfolk Canyon seeps, where samples were acquired in 2012-2013, 2015, and 2017. White circles indicate seep sites identified by Skarke et al. (2014), and the names on the outer shelf indicate the major shelf-breaking canyons. The inset shows the location of the map within the broader context of the margin. Multibeam data and bottom photographs of A) Baltimore (BCS) and B) Norfolk (NCS) seeps with points representing the samples collected from seeps for stable isotope analyses. Red square = mussels, white square = microbial mat, white circle = other fauna, white triangle = sediment, and white diamond = POM. Bottom images represent the types of habitats encountered at both sites, including large and small mussel patches.

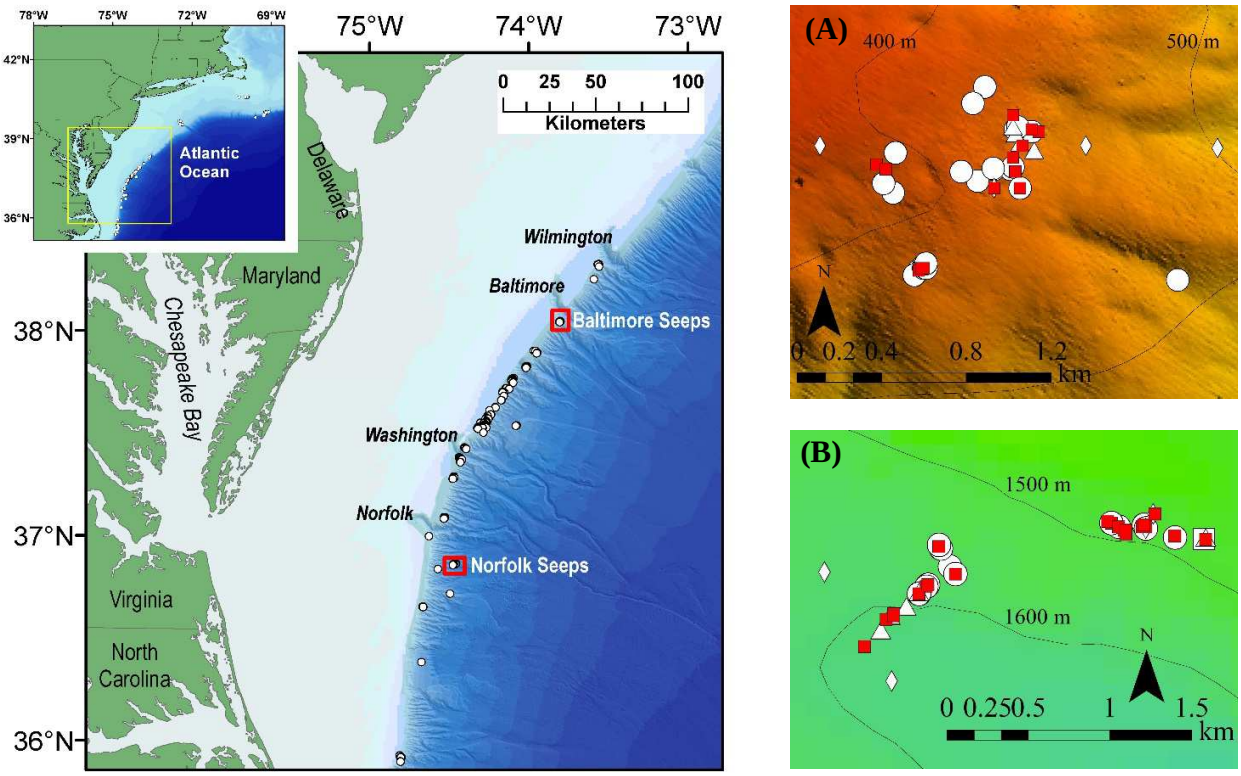

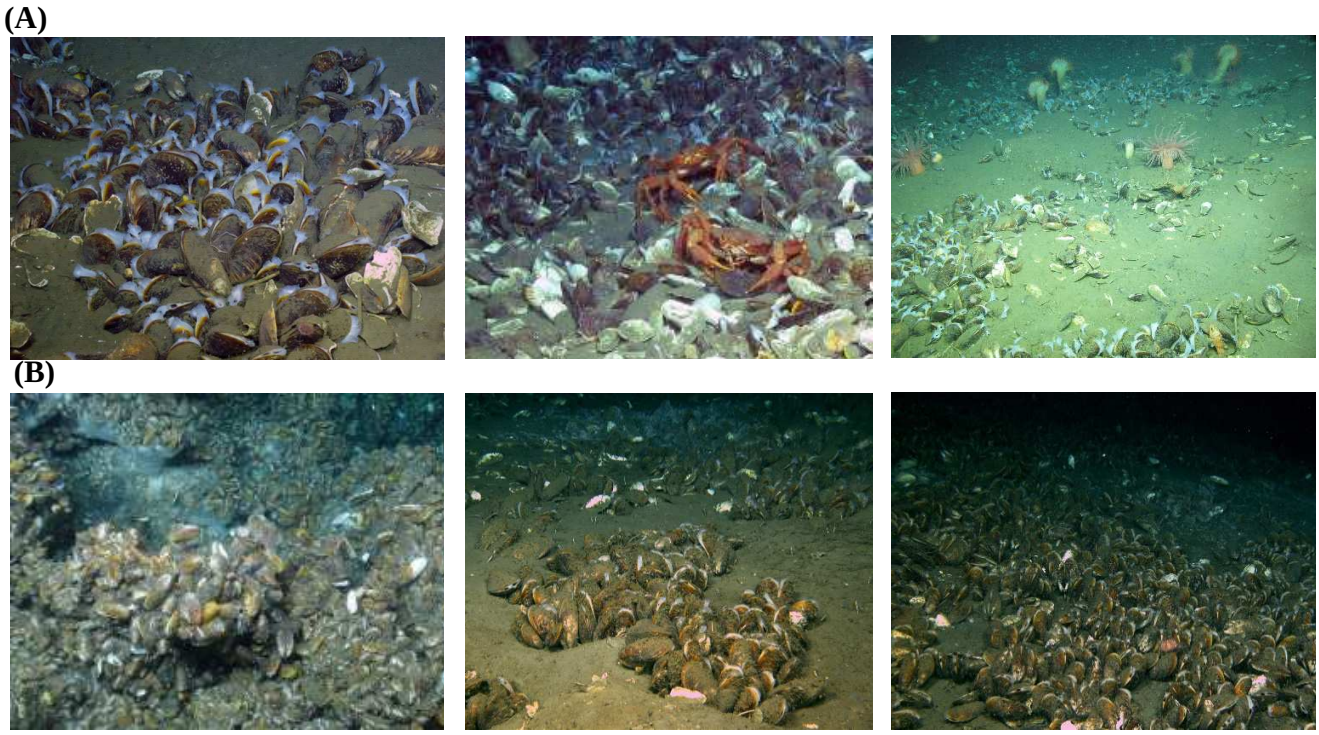

Figure 2. Average $\delta^{13}C$ versus $\delta^{15}N$ (‰ ± SD) for POM, microbial mat, consumers, and surface sediments (0-2 cm) collected from (A) Baltimore and (B) Norfolk seeps. Colors represent general feeding strategies, with red = benthos, blue = water column, purple = mixed diets, white = utilize chemosynthetic material, green = unknown. Symbols represent different feeding groups. For POM, B=bottom, M=midwater, and S=surface. For mussels, Bc=*Bathymodiolus childressi*, Bh=*B. heckerae*, G=gill, Ma=mantle, Mu=muscle.

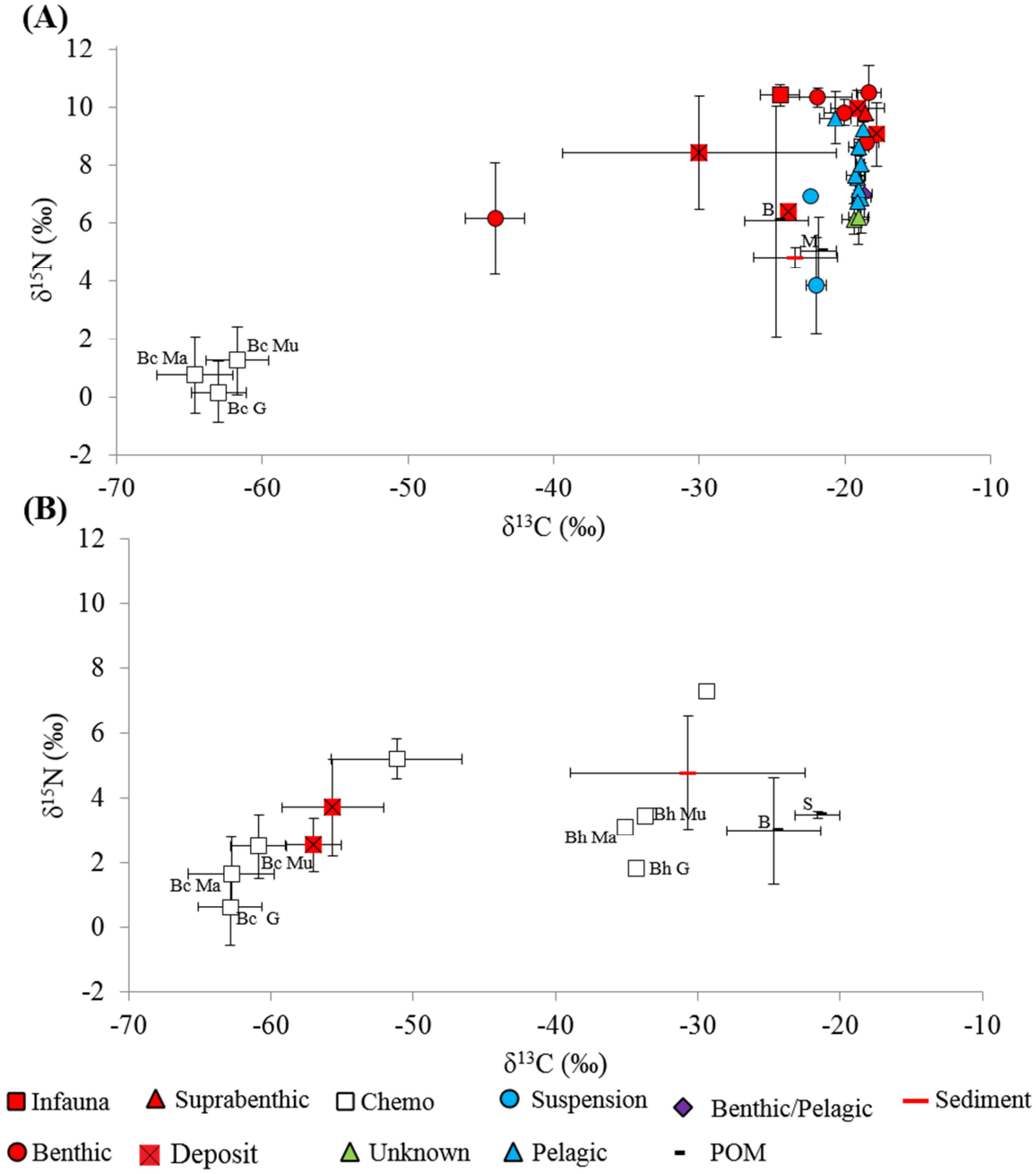

Figure 3. Averaged linear mixed model predictions from the averaged top model for $\delta^{13}C$, $\delta^{15}N$, and $\delta^{34}S$. The top models for $\delta^{13}C$ and $\delta^{15}N$ contained all three variables (Tissue, Live, and Year), whereas the model for $\delta^{34}S$ was built using data from only 2013. Vertical bars represent 95% confidence intervals.

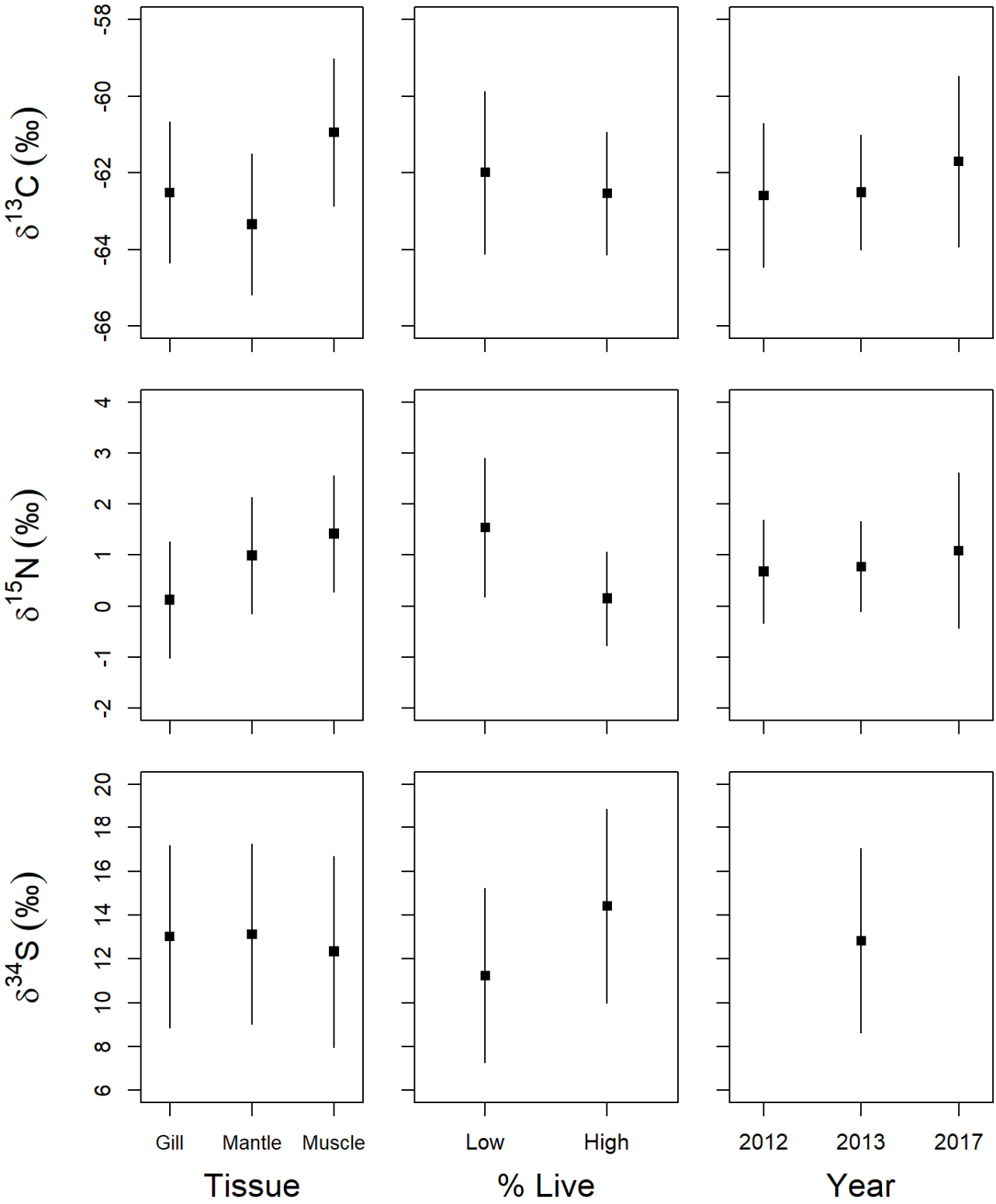

Figure 4. Visualization of the seep environments at BCS and NCS and the effect of live mussel density on stable isotope composition of *Bathymodiolus childressi* mussels based on LMM results.

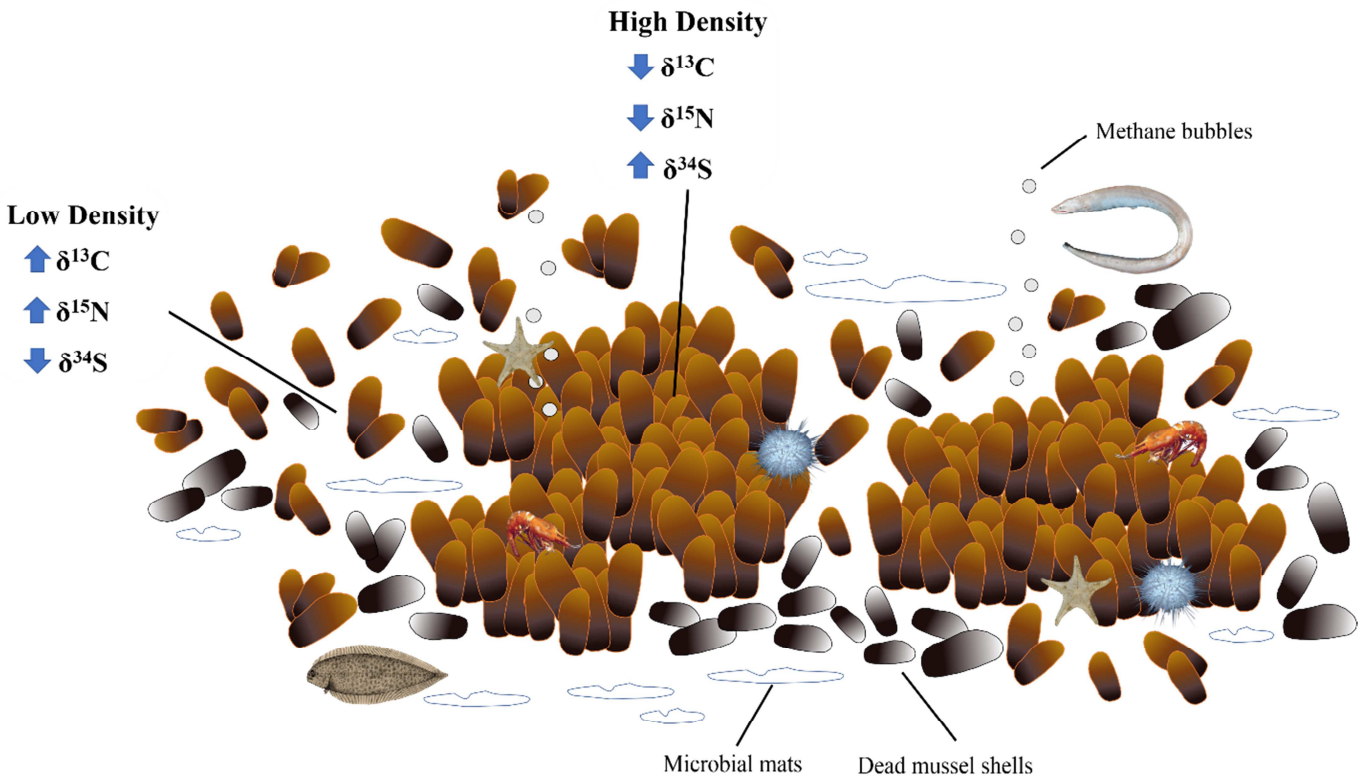

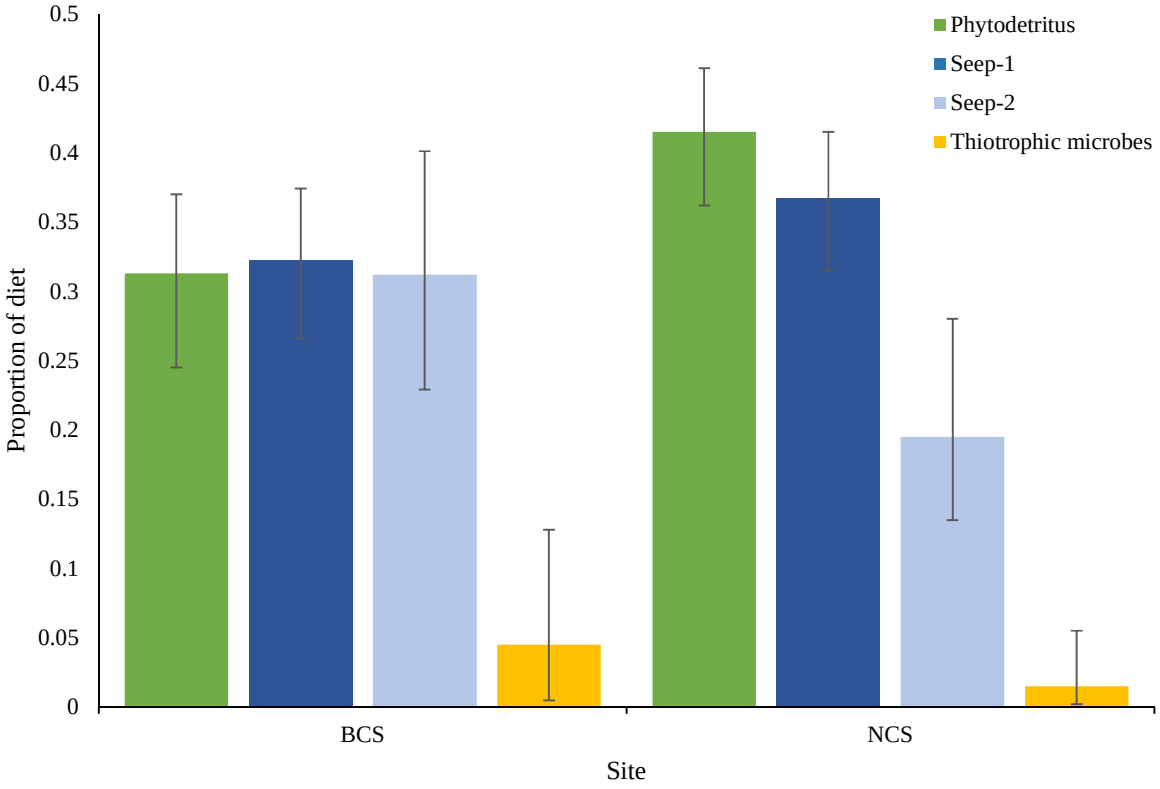

Figure 5. MixSIAR results based on *Bathymodiolus childressi* isotope data illustrating the relative contribution (median ± 95% credible intervals) of 4 sources to muscle tissue by site.

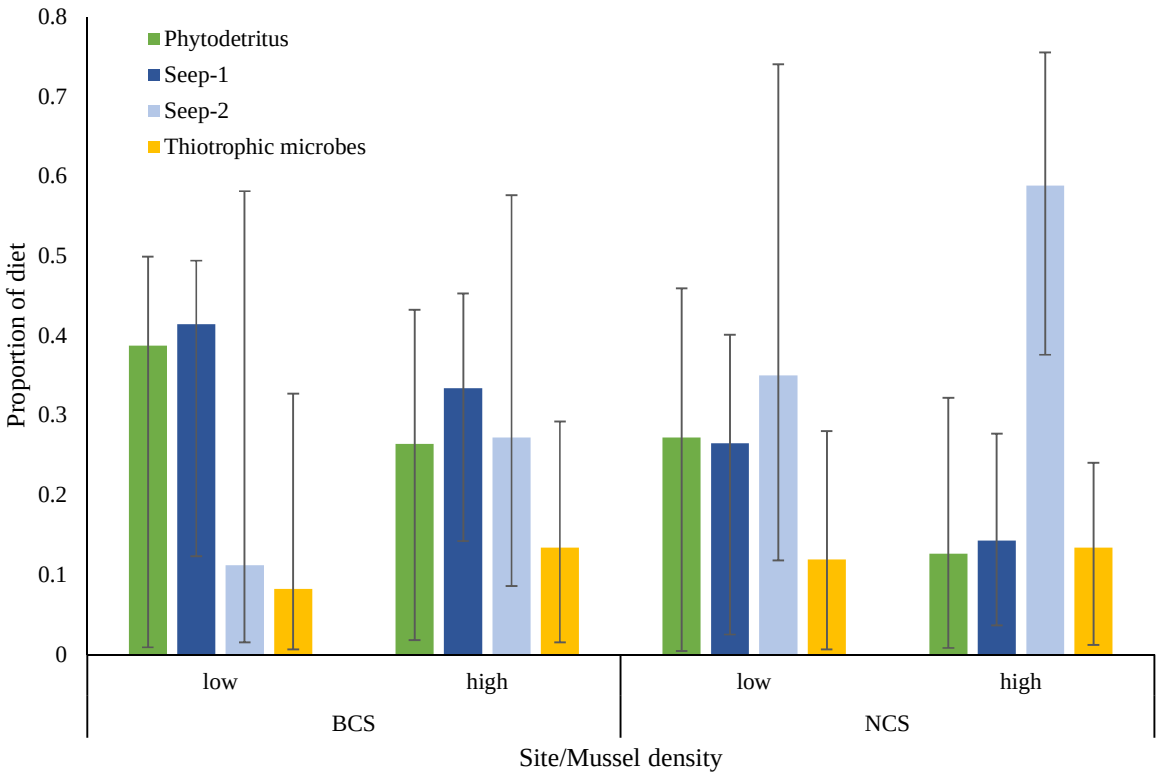

Figure 6. MixSIAR results based on *Bathymodiolus childressi* $\delta^{13}C$ and $\delta^{15}N$ isotope data illustrating the relative contribution (median ± 95% credible intervals) of 4 sources to muscle tissues at each site based on mussel density categories (low and high).

Supplemental Table 1. Collection locations for isotope samples. Bin refers to the sample container: BK = basket, BBB = biobox bow, BBP = biobox port, BBS = biobox starboard, BBC = biobox center, EK = Ekman sampler, Q = quiver, KQ = Kellogg quiver, S = suction, PC = push core, NB = niskin bottle, NA = Information not available. # Ind refers to the number of individual specimens sampled for stable isotope analysis, whereas as n is the number of isotope samples taken.

Seep	Year	Station	Bin	Latitude	Longitude	Depth (m)	#Ind	n
Baltimore	Aug2012	ROV-2012-NF-07	BBB	38.0437	-73.8259	403	1	3
			BBC	38.0435	-73.8261	401	2	2
			BBC	38.0438	-73.8258	402	3	9
			Q3	38.0438	-73.8256	403	1	1
			Q4	38.0440	-73.8256	401	2	2
			S2	38.0437	-73.8259	403	9	9
			S3A	38.0438	-73.8256	402	2	2
			S3B	38.0438	-73.8257	402	9	11
			S5	38.0439	-73.8257	401	2	2
			S7	38.0439	-73.8256	401	10	10
		ROV-2012-NF-08	BBB	38.0490	-73.8215	410	3	9
			BBC	38.0496	-73.8208	420	1	3
			Q3	38.0438	-73.8257	402	1	1
			S1	38.0472	-73.8216	408	29	33
			S3A	38.0497	-73.8211	421	1	3
			S3B	38.0496	-73.8211	420	1	1
			S4	38.0438	-73.8256	402	16	16
			S8	38.0490	-73.8215	411	15	42
	Sep 2012	ROV-2012-NF-14	S1	38.0433	-73.8149	496	17	17
			S2	38.0498	-73.8217	406	3	3
			S4	38.0487	-73.8269	359	2	2
			S5	38.0474	-73.8274	374	5	5
			S6	38.0515	-73.8231	381	4	4
			S7	38.0508	-73.8236	382	4	4
			S8	38.0497	-73.8218	403	1	1
			NA	38.0498	-73.8217	406	2	2
	May 2013	ROV-2013-RB-689	BK	38.0479	-73.8241	389	3	3
			BBB	38.0482	-73.8277	363	6	18
			BBP	38.0485	-73.8219	400	5	15
			BBS	38.0479	-73.8218	400	5	14
			EK	38.0503	-73.8219	401	4	12
			KQ4	38.0480	-73.8273	365	1	3
			NA	38.0479	-73.8241	389	1	1

			NB	38.0497	-73.8219	399	1	1
			Q10	38.0472	-73.8265	373	3	3
			S black	38.0480	-73.8220	406	4	4
			S blue	38.0475	-73.8234	387	3	3
			S green	38.0481	-73.8219	398	2	2
	Aug 2013	NF-2013-011	NB	38.0489	-73.8301	29-335	2	2
		NF-2013-015	NB	38.0490	-73.8188	25	1	1
		NF-2013-017	NB	38.0489	-73.8132	28-508	2	2
	July 2015	AT29-04-4807	PC04	38.0488	-73.8210	419	1	1
			PC10	38.0490	-73.8216	406	1	1
		AT29-04-4808	PC01	38.0495	-73.8218	396	1	1
			PC10	38.0498	-73.8219	399	1	1
	May 2017	HRS1704-GEX06-075	BBP	38.0472	-73.8227	393	7	21
		HRS1704-GEX06-076	NB	38.0472	-73.8227	392	1	1
		HRS1704-GEX06-090	Q	38.0480	-73.8227	394	7	7
Norfolk	May 2013	RB-2013-031	NB	36.8630	-74.4903	5-1603	2	2
		RB-2013-084	NB	36.8690	-74.4939	3-1570	2	2
		ROV-2013-RB-682	BBC	36.8704	-74.4876	1536	2	4
			BBP	36.8664	-74.4905	1593	2	4
			BBS	36.8649	-74.4917	1611	2	4
			PC03	36.8658	-74.4908	1602	1	1
			PC04	36.8671	-74.4894	1585	1	1
			PC05	36.8679	-74.4887	1576	1	1
			PC06	36.8666	-74.4903	1589	1	1
			Q10A	36.8667	-74.4901	1588	1	2
			Q11A	36.8682	-74.4883	1567	6	11
			Q18A	36.8678	-74.4887	1576	2	3
			Q18B	36.8678	-74.4887	1576	4	8
			Q01A	36.8683	-74.4882	1565	8	15
			Q01B	36.8683	-74.4882	1564	1	1
			Q02A	36.8683	-74.4882	1565	1	2
			Q03A	36.8705	-74.4876	1536	1	1
			Q06A	36.8689	-74.4867	1548	1	2
			Q06B	36.8689	-74.4867	1548	1	1
			QK05	36.8666	-74.4901	1590	1	2
			S black	36.8693	-74.4870	1531	5	5
			S yellow	36.8703	-74.4875	1533	2	2
		ROV-2013-RB-683	NA	36.8711	-74.4773	1484	7	21
			NB	36.8714	-74.4762	1480	1	1

		PC	36.8708	-74.4730	1457	1	1
		PC08	36.8709	-74.4729	1457	1	1
		Q01	36.8713	-74.4774	1487	1	2
		Q02A	36.8709	-74.4746	1476	3	3
		Q02B	36.8708	-74.4729	1456	4	8
		Q04	36.8710	-74.4746	1476	2	4
		Q05	36.8718	-74.4783	1485	5	10
		Q06	36.8714	-74.4762	1480	5	5
		Q07A	36.8715	-74.4777	1487	3	5
		Q07B	36.8716	-74.4763	1483	2	3
		Q08	36.8713	-74.4773	1487	5	10
		Q15	36.8710	-74.4746	1476	2	4
		Q16	36.8715	-74.4763	1483	1	1
		Q17A	36.8717	-74.4781	1487	5	13
		Q17B	36.8717	-74.4781	1487	1	1
		Q18	36.8715	-74.4777	1487	2	2
May 2017	HRS1704-GEX03-009	Q7	36.8715	-74.4762	1482	7	21
	HRS1704-GEX03-011	BBP	36.8715	-744764	1491	9	27
	HRS1704-GEX03-022	NB	36.8722	-74.4758	1492	1	1
	HRS1704-GEX03-023	BBS	36.8722	-74.4757	1494	11	33

Supplemental Table 2. Model selection table for $\delta^{13}C$ linear mixed model set. The random effect in the model was a random intercept with collection (bin) nested within site (Baltimore or Norfolk). The full model had a three-way interaction between all the variables: Live (live mussel cover; high or low), Tissue (gill, mantle, or muscle), and Year (2012, 2013, or 2017; treated as categorical variables). If a model contained an interaction term, all lower-order terms in that interaction were also included in the model. The column ω shows the Akaike weight for each model, R^2(m) shows the marginal R^2, and R^2(c) shows the conditional R^2.

Model	**Parameters**	**AICc**	**ΔAICc**	**ω**	**R^2(m)**	**R^2(c)**
Full (Live x Tissue x Year)	21	1534.13	0.00	0.45	0.21	0.45
Live x Year + Tissue x Year	15	1535.37	1.24	0.24	0.21	0.45
Live x Tissue + Live x Year + Tissue x Year	17	1536.90	2.77	0.11	0.21	0.45
Live + Tissue x Year	13	1537.07	2.94	0.10	0.20	0.43
Live x Tissue + Tissue x Year	15	1538.66	4.53	0.05	0.20	0.43
Tissue x Year	12	1539.28	5.15	0.03	0.16	0.40
Tissue + Live x Year	11	1551.39	17.25	0.00	0.17	0.42
Live x Tissue + Live x Year	13	1552.02	17.89	0.00	0.17	0.42
Live + Tissue + Year	9	1552.97	18.84	0.00	0.16	0.40
Tissue	6	1553.24	19.11	0.00	0.12	0.34
Live + Tissue	7	1553.57	19.44	0.00	0.13	0.35
Year + Live x Tissue	11	1553.64	19.51	0.00	0.17	0.40
Live x Tissue	9	1554.22	20.08	0.00	0.13	0.35
Tissue + Year	8	1555.03	20.89	0.00	0.13	0.36
Live x Year	9	1593.96	59.83	0.00	0.08	0.27
Live + Year	7	1595.70	61.57	0.00	0.08	0.25
Year	6	1598.81	64.68	0.00	0.02	0.21
Null	4	1599.27	65.14	0.00	0.00	0.19
Live	5	1599.81	65.68	0.00	0.01	0.18

Supplemental Table 3. Model selection table for $\delta^{15}N$ linear mixed model set. The random effect in the model was a random intercept with collection (bin) nested within site (Baltimore or Norfolk). The full model had a three-way interaction between all the variables: Live (live mussel cover; high or low), Tissue (gill, mantle, or muscle), and Year (2012, 2013, or 2017; treated as categorical variables). If a model contained an interaction term, all lower-order terms in that interaction were also included in the model. The column ω shows the Akaike weight for each model, R^2(m) shows the marginal R^2, and R^2(c) shows the conditional R^2.

Model	**Parameters**	**AICc**	**ΔAICc**	**ω**	**R^2(m)**	**R^2(c)**
Tissue + Live x Year	11	945.81	0.00	0.88	0.32	0.76
Live x Tissue + Live x Year	13	950.99	5.19	0.07	0.32	0.76
Live x Year + Tissue x Year	15	951.60	5.79	0.05	0.32	0.77
Live x Tissue + Live x Year + Tissue x Year	17	957.05	11.24	0.00	0.32	0.77
Full (Live x Tissue x Year)	21	962.67	16.86	0.00	0.32	0.76
Live + Tissue + Year	9	964.65	18.84	0.00	0.35	0.72
Year + Live x Tissue	11	969.67	23.86	0.00	0.35	0.72
Live + Tissue	7	970.55	24.75	0.00	0.20	0.60
Live + Tissue x Year	13	970.63	24.82	0.00	0.35	0.72
Live x Tissue	9	975.55	29.74	0.00	0.20	0.60
Live x Tissue + Tissue x Year	15	975.85	30.04	0.00	0.35	0.72
Tissue	6	976.12	30.31	0.00	0.17	0.52
Tissue + Year	8	981.11	35.30	0.00	0.18	0.53
Tissue x Year	12	986.93	41.12	0.00	0.18	0.53
Live x Year	9	1051.16	105.35	0.00	0.24	0.60
Live + Year	7	1062.71	116.90	0.00	0.21	0.55
Live	5	1067.87	122.06	0.00	0.03	0.40
Null	4	1069.99	124.18	0.00	0.00	0.35
Year	6	1074.37	128.56	0.00	0.01	0.34

Supplemental Table 4. Model selection table for $\delta^{34}S$ linear mixed model set. The random effect in the model was a random intercept with collection (bin) nested within site (Baltimore or Norfolk). The full model had an interaction between both the variables: Live (live mussel cover; high or low) and Tissue (gill, mantle, or muscle). Year was not included because of inadequate sample size in 2012 (n=0) and 2017 (n=3). If a model contained an interaction term, all lower-order terms in that interaction were also included in the model. The column ω shows the Akaike weight for each model, R^2(m) shows the marginal R^2, and R^2(c) shows the conditional R^2.

Model	**Parameters**	**AICc**	**ΔAICc**	**ω**	**R^2(m)**	**R^2(c)**
Full (Live x Tissue)	9	295.35	0.00	0.37	0.13	0.77
Live	5	295.84	0.49	0.29	0.11	0.77
Live + Tissue	7	296.52	1.17	0.21	0.12	0.77
Null	4	298.76	3.41	0.07	0.00	0.79
Tissue	6	298.99	3.65	0.06	0.01	0.78

Supplemental Table 5. Skewness of $\delta^{13}C$, $\delta^{15}N$, and $\delta^{34}S$ for different tissue types sampled from the mussels *Bathymodiolus childressi* collected at BCS and NCS. Negative values are skewed left and positive values are skewed right. The p-values were calculated using the D'Agostino test for skewness, and significant values ($p < 0.05$) are shown in bold.

	Baltimore Canyon			Norfolk Canyon		
Tissue	$\delta^{13}C$	$\delta^{15}N$	$\delta^{34}S$	$\delta^{13}C$	$\delta^{15}N$	$\delta^{34}S$
Gill	-0.04	**0.89**	**-1.63**	**-1.27**	0.04	0.10
	p = 0.899	p = 0.008	p = 0.007	p < 0.001	p = 0.875	p = 0.855
Mantle	**-0.85**	**1.44**	**-1.23**	0.21	-0.13	-0.76
	p = 0.012	p < 0.001	p = 0.036	p = 0.405	p = 0.605	p = 0.157
Muscle	**-1.25**	0.30	**-1.47**	-0.55	**-0.81**	0.34
	p = 0.001	p = 0.322	p = 0.014	p = 0.131	p = 0.035	p = 0.544

Supplemental Table 6. Isotope niche area (‰^{2}) estimates (sample size-corrected standard ellipse area, SEA_C; and Bayesian SEA, SEA_B), including 95% credible intervals calculated from the isotopic values from different mussel tissues as a function of mussel density at BCS and NCS. Bold values were significantly different ($p < 0.05$).

		N	SEA_C	SEA_B	95% CI	
Baltimore						
Gill	high	35	4.75	4.49	3.21	6.36
	low	19	6.90	6.21	3.93	10.11
Mantle	high	34	8.96	8.55	5.94	12.04
	low	18	10.81	9.46	6.12	16.15
Muscle	high	35	7.52	7.12	5.04	10.03
	low	19	6.90	6.55	3.86	10.27
Norfolk						
Gill	high	69	9.24	**9.02**	7.13	11.49
	low	18	2.25	**2.10**	1.27	3.41
Mantle	high	68	10.95	10.65	8.40	13.51
	low	18	7.41	6.69	4.05	10.95
Muscle	high	26	4.34	4.00	2.74	6.16
	low	11	3.39	2.82	1.55	5.69

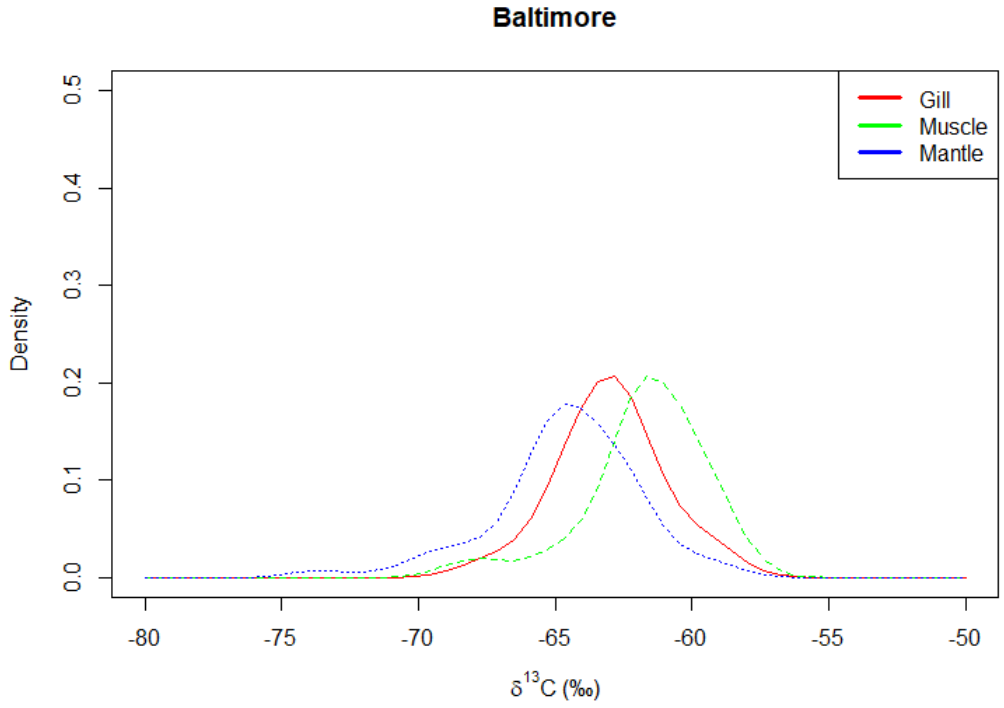
Baltimore
Gill
Muscle
Mantle
Density
0.0
0.1
0.2
0.3
0.4
0.5
-80
-75
-70
-65
-60
-55
-50
δ13C (‰)

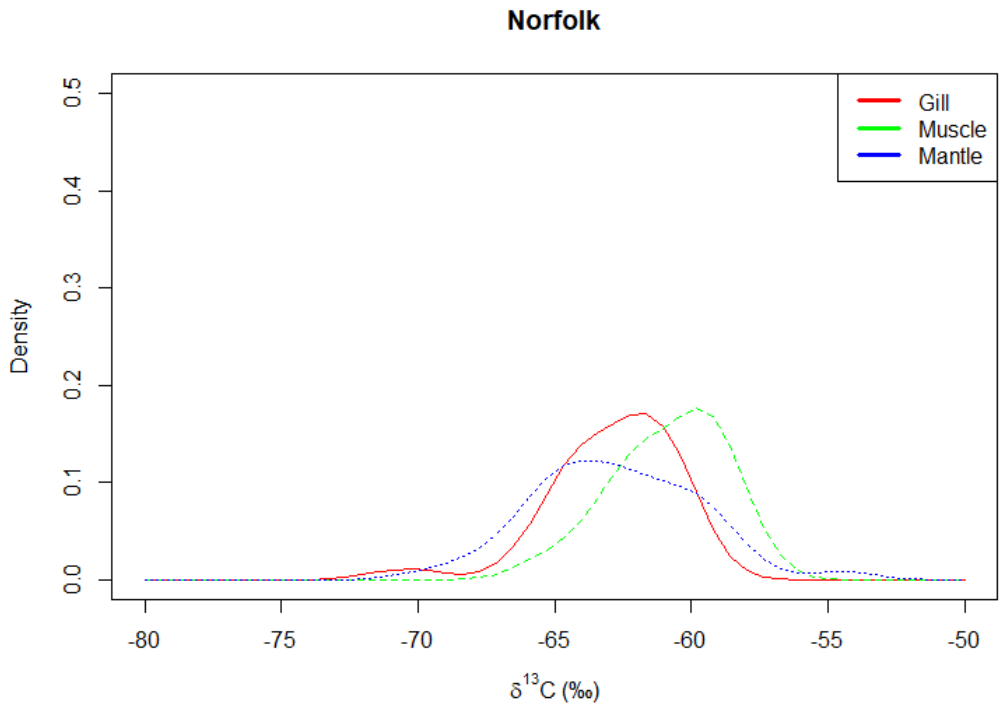
Norfolk
Gill
Muscle
Mantle
Density
0.0
0.1
0.2
0.3
0.4
0.5
-80
-75
-70
-65
-60
-55
-50
δ13C (‰)

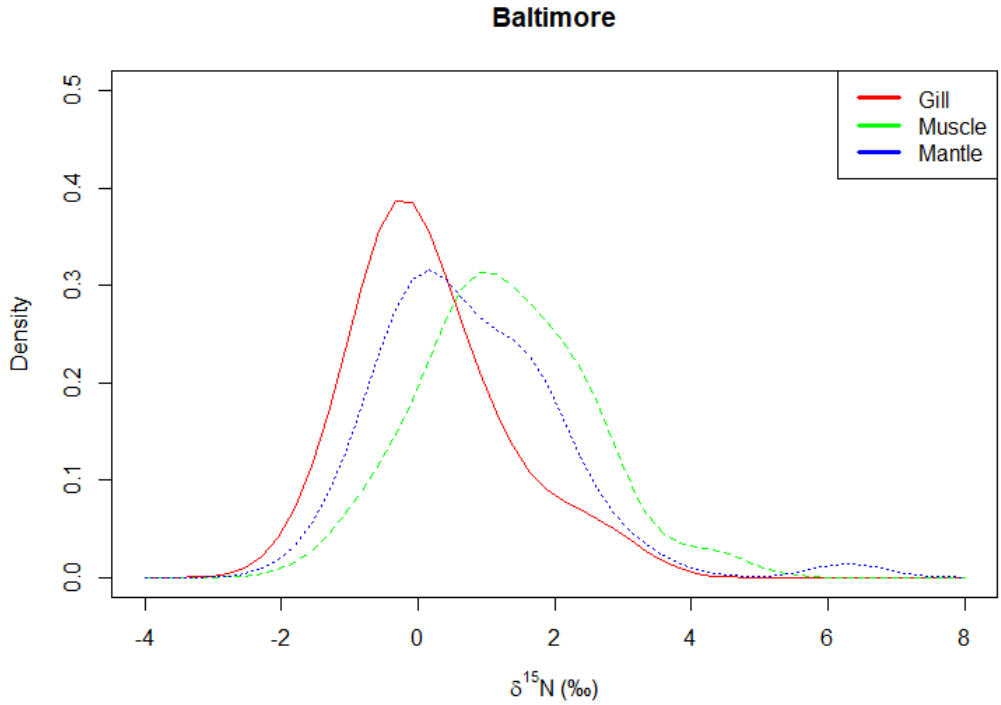
Baltimore
Gill
Muscle
Mantle
Density
0.0
0.1
0.2
0.3
0.4
0.5
-4
-2
0
2
4
6
8
δ15N (‰)

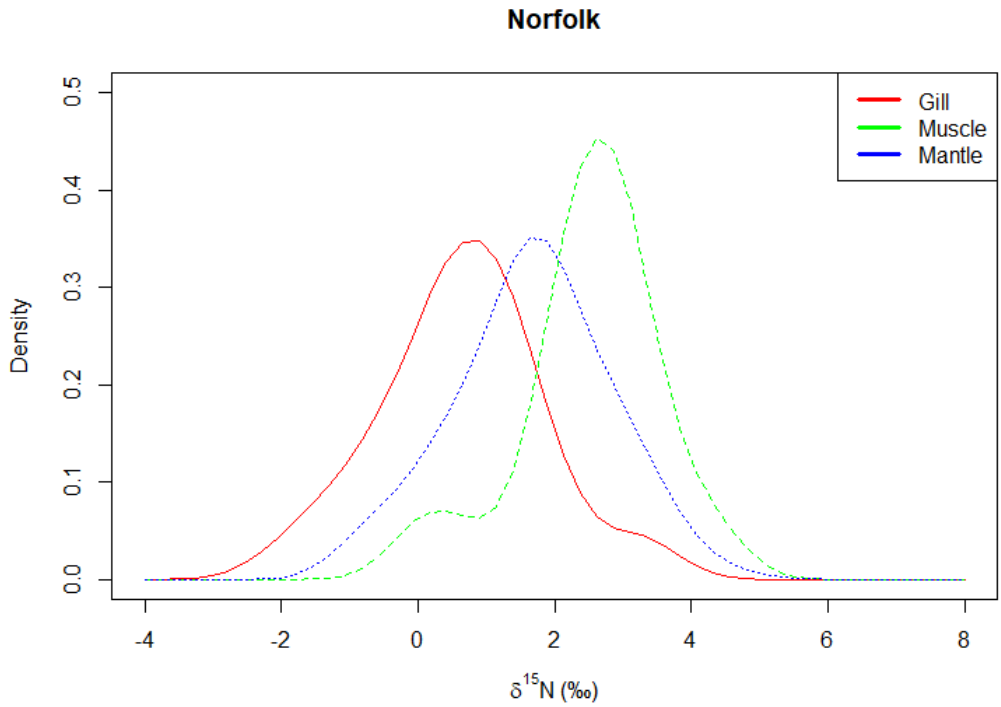
Norfolk
Gill
Muscle
Mantle
Density
0.0
0.1
0.2
0.3
0.4
0.5
-4
-2
0
2
4
6
8
δ15N (‰)

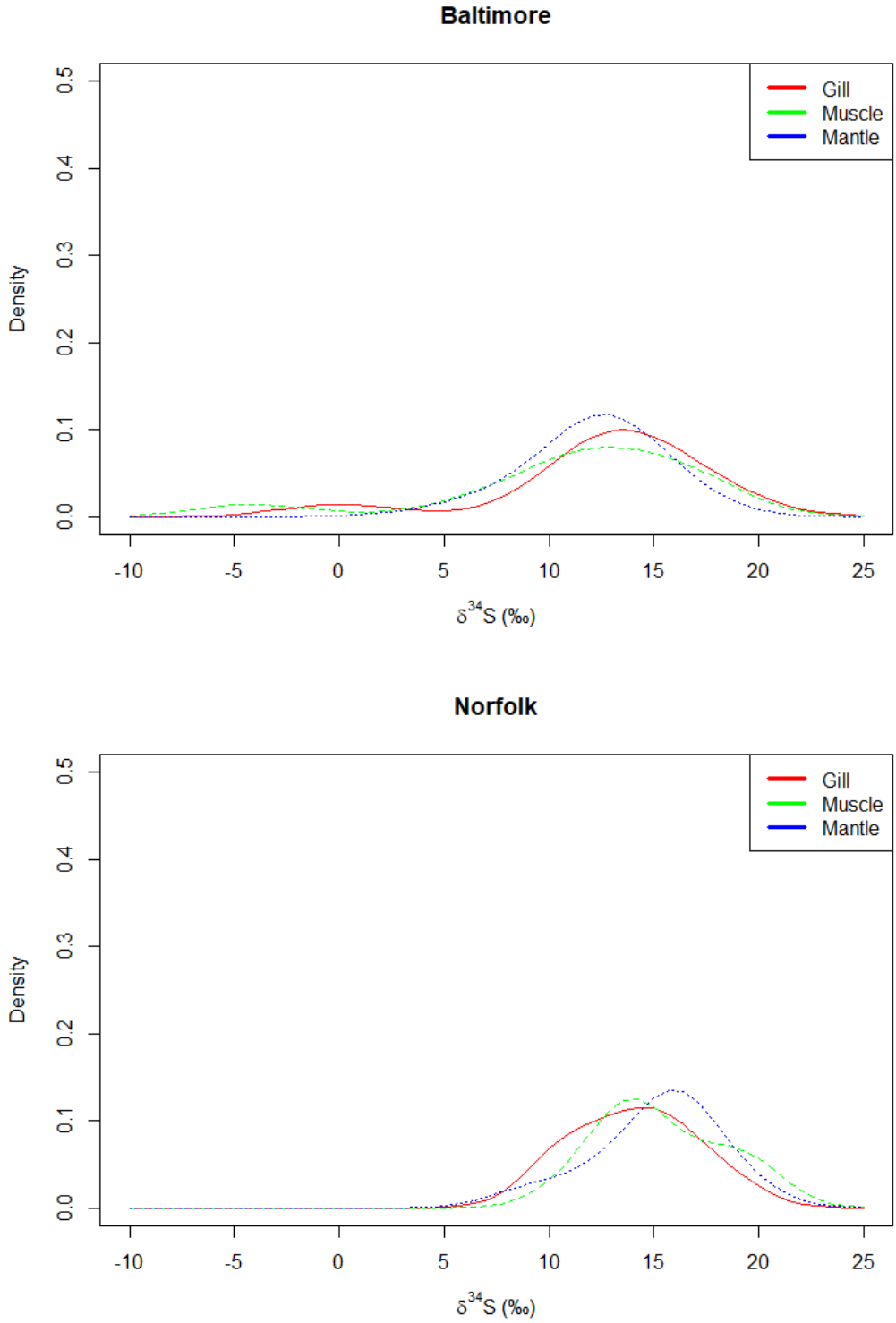

Supplemental Figure 1: Kernel density plots of stable isotope values from *Bathymodiolus childressi* tissue, for Baltimore (BCS) and Norfolk (NCS).

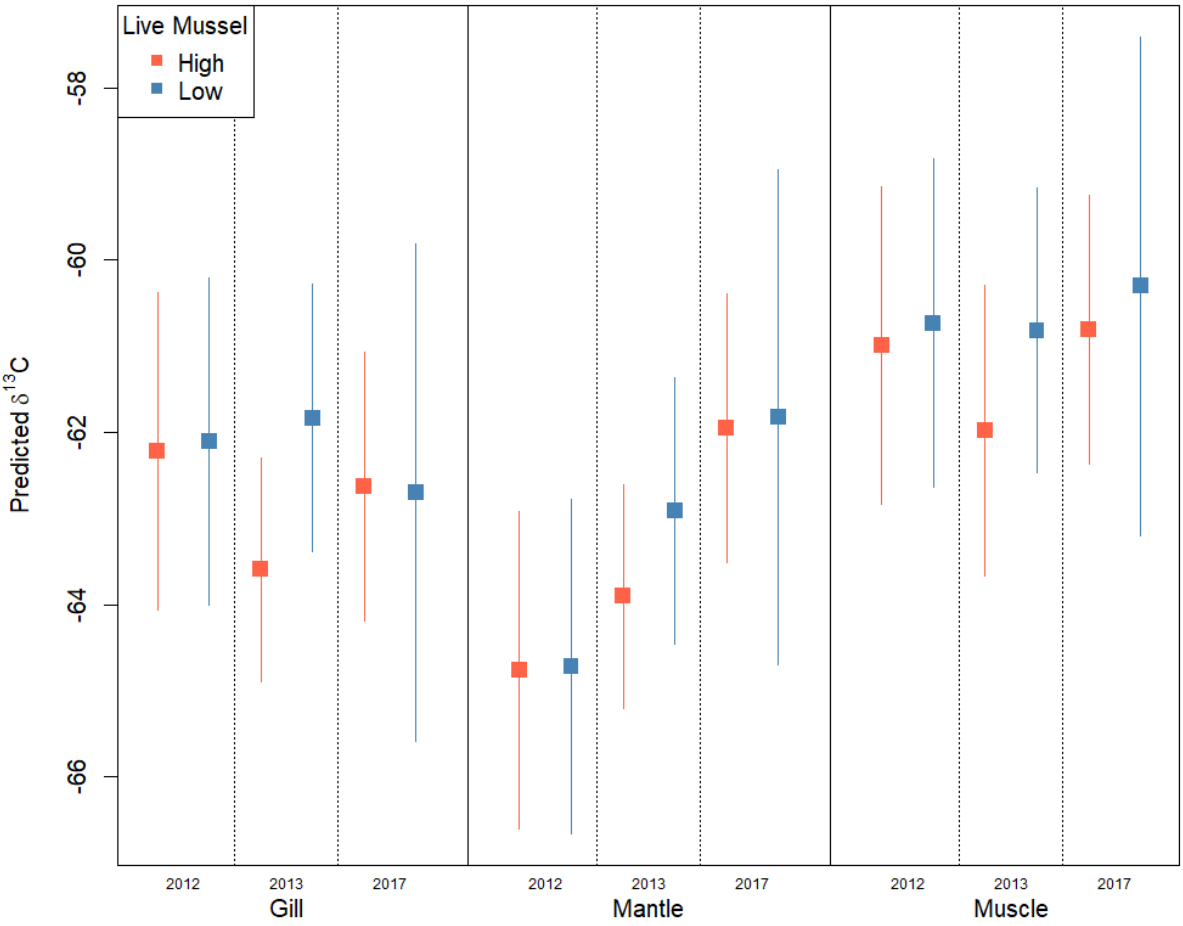
Live Mussel
High
Low
Predicted δ13C
-58
-60
-62
-64
-66
2012
2013
2017
Gill
2012
2013
2017
Mantle
2012
2013
2017
Muscle

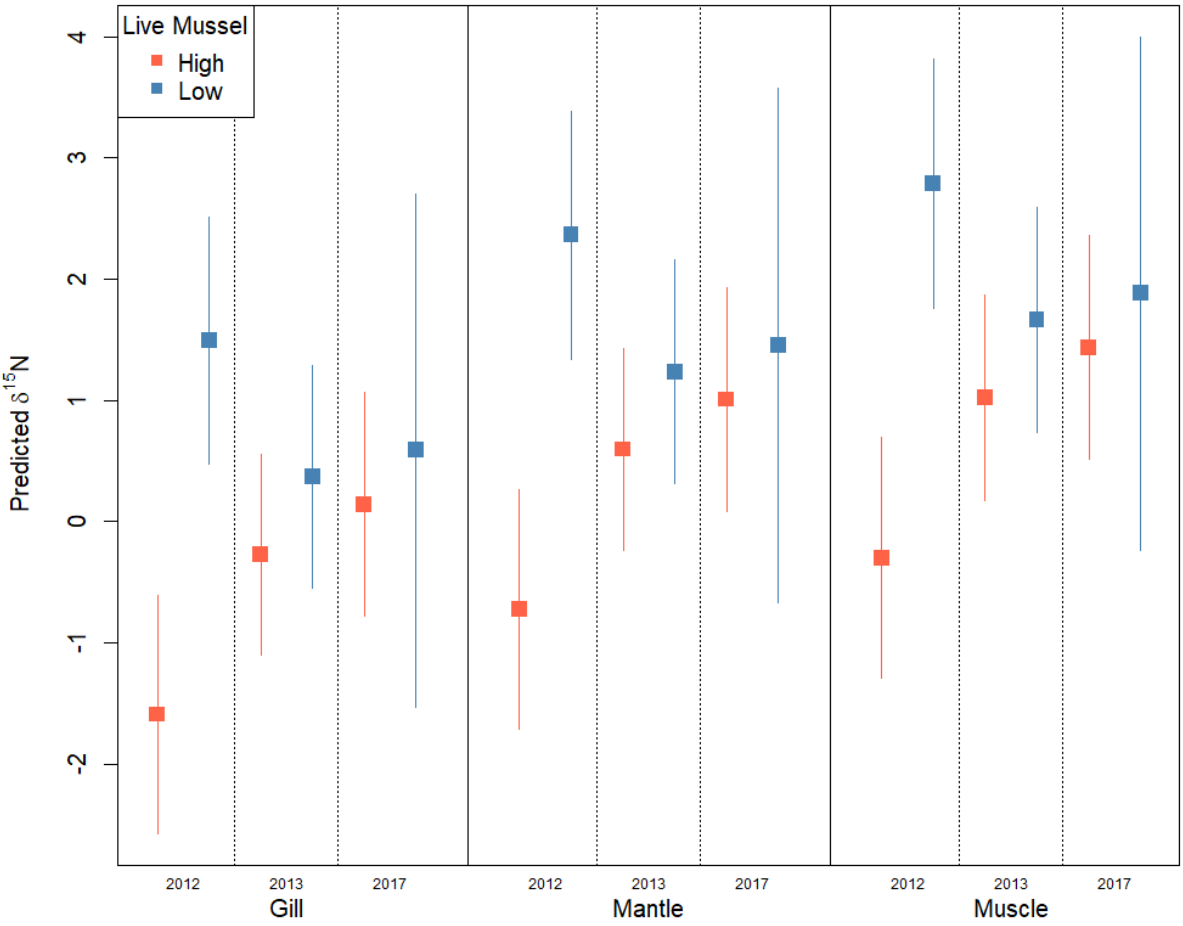
Live Mussel
High
Low
Predicted δ15N
4
3
2
1
0
-1
-2
2012
2013
2017
Gill
2012
2013
2017
Mantle
2012
2013
2017
Muscle

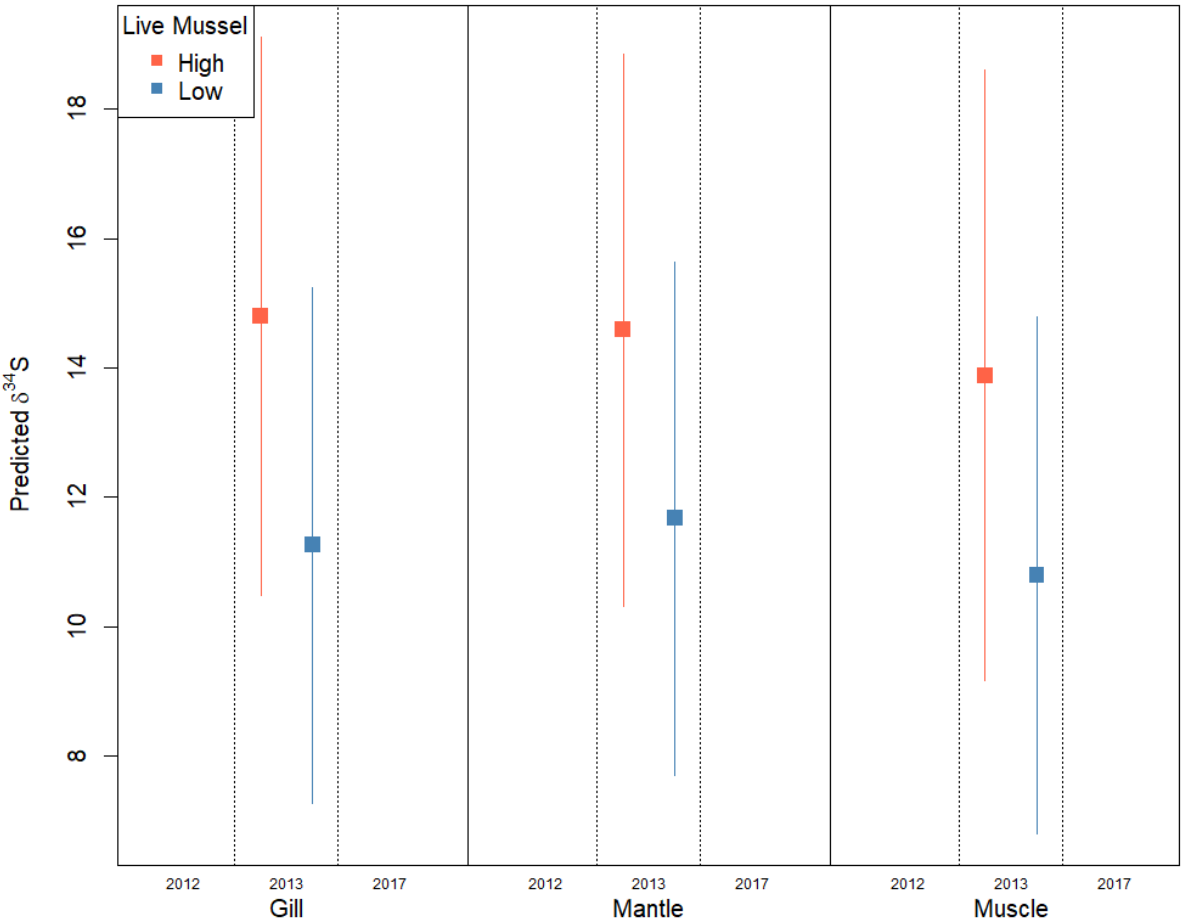

Supplemental Figure 2. LMM model predictions for $\delta^{13}C$, $\delta^{15}N$, and $\delta^{34}S$ versus tissue and collection year in high (red) and low (blue) density mussel beds.

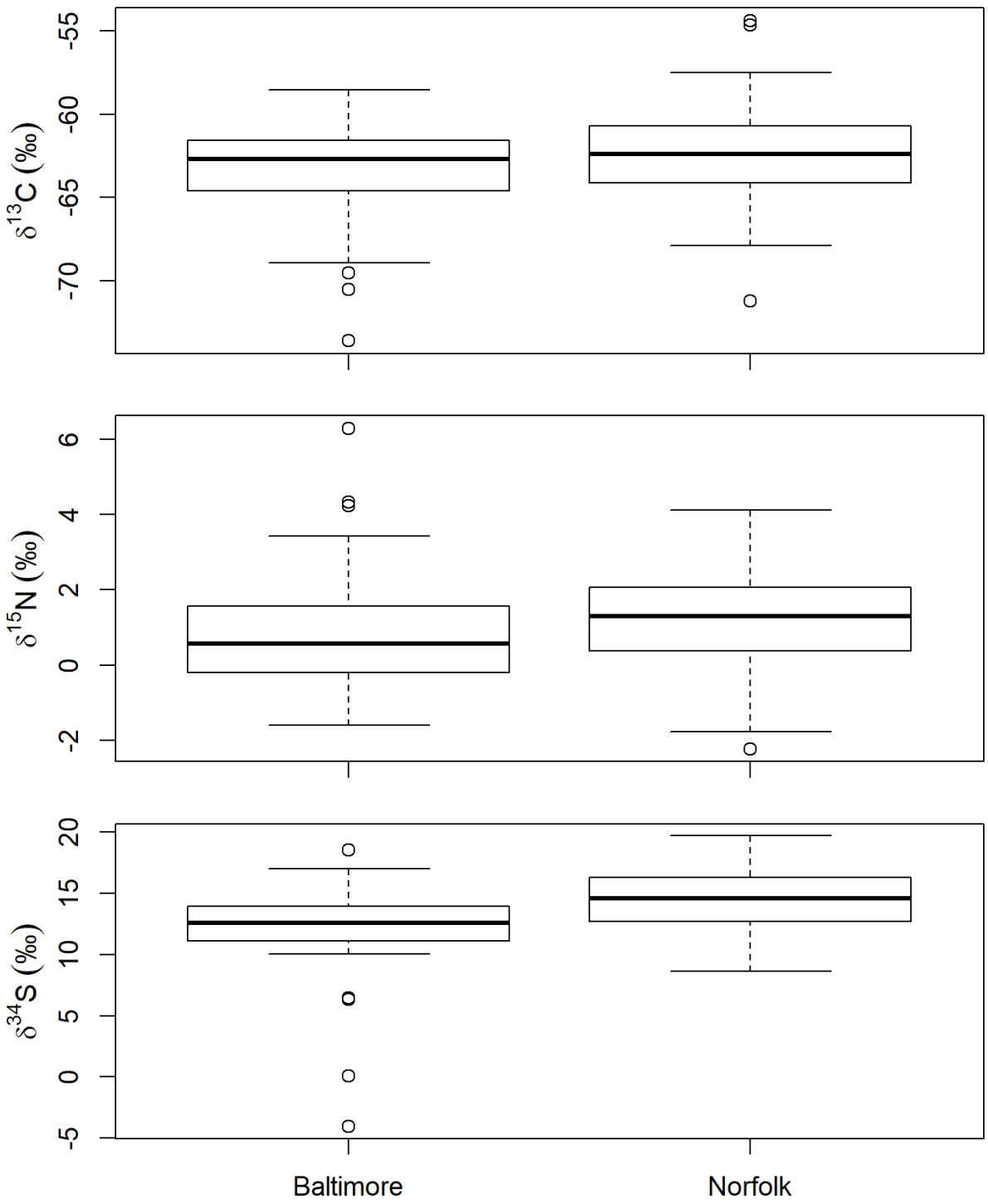

Supplemental Figure 3. Boxplots of $\delta^{13}C$, $\delta^{15}N$, and $\delta^{34}S$ at the two study sites (Baltimore Canyon and Norfolk Canyon seeps).

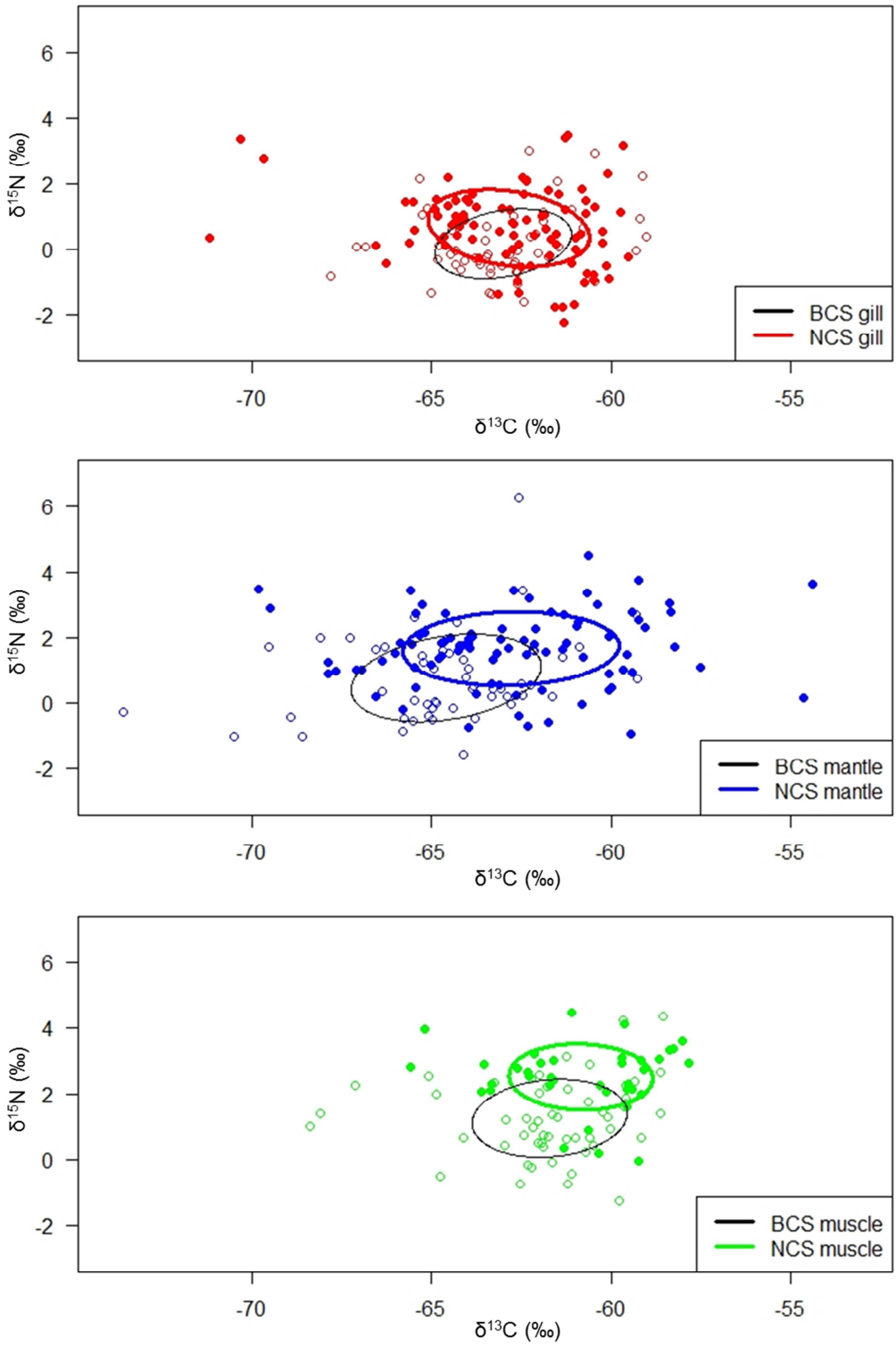

Supplemental Figure 4. Raw mussel isotope data from BCS (open symbols) and NCS (closed symbols) for each of the different tissues and associated standard ellipse areas (SEA_C) for gill, mantle, and muscle tissues. SEA_C values are included in Table 3.

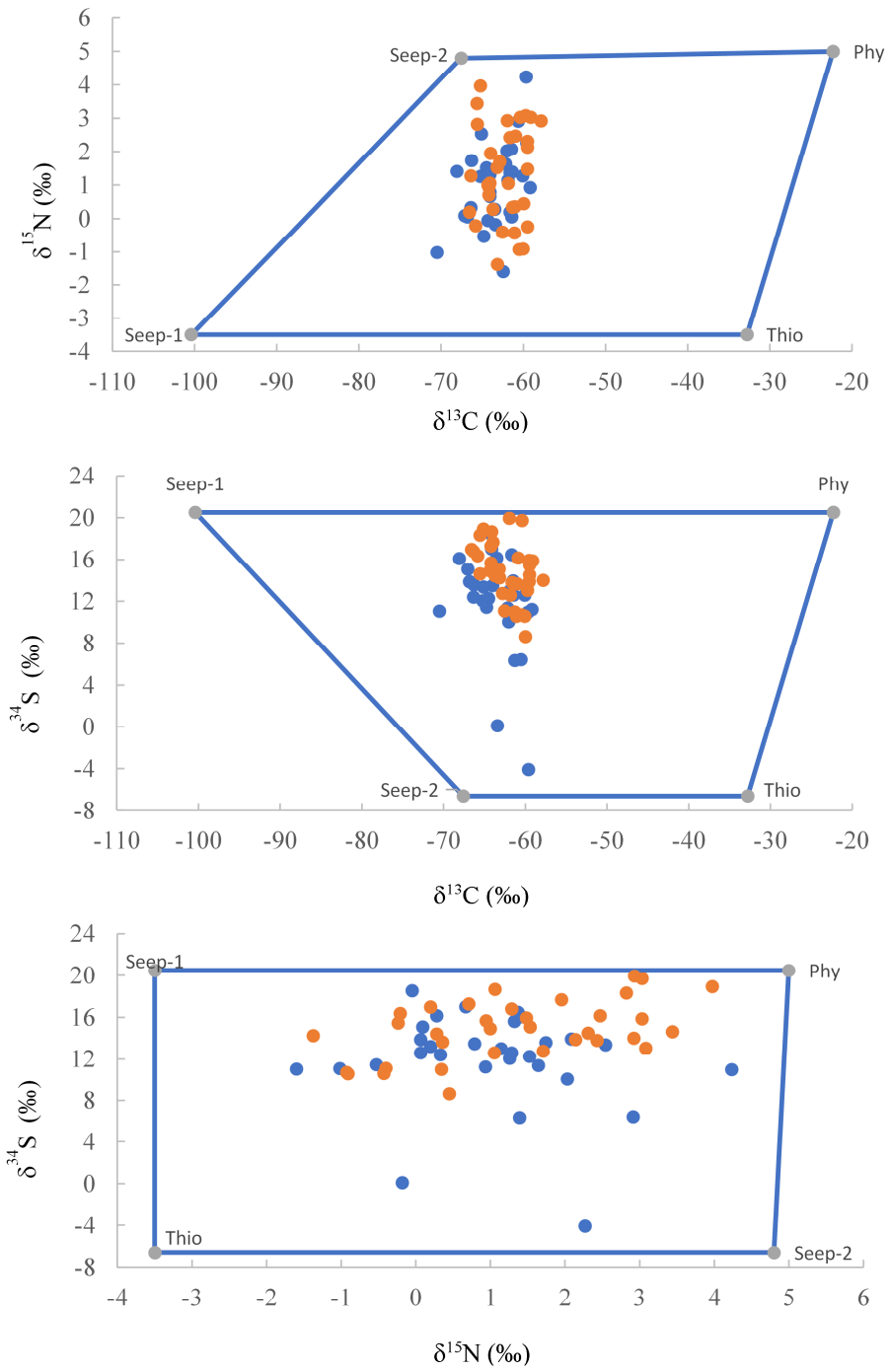

Supplemental Figure 5. Graphical representation of polygons fitted around mussel isotope data from NCS (orange) and BCS (blue) with the vertices (grey) representing trophic resources (Table 5). Phy= phytodetritus, Thio = thiotrophic microbes